A $^{40}Ar/^{39}Ar$ and U–Pb timescale for the Cretaceous Western Interior Basin, North America

Brad S. Singer[1]*, Brian R. Jicha[1], David A. Sawyer[2], Ireneusz Walaszczyk[3], Neil Landman[4], Bradley B. Sageman[5] and Kevin C. McKinney[6]

[1]Department of Geoscience, University of Wisconsin-Madison, 1215 West Dayton Street, Madison, WI 53706, USA

[2]University of Colorado, Boulder; 955 Adams Street, Denver, CO 80206, USA

[3]Faculty of Geology, University of Warsaw, Al. Zwirki i Wigury 92, PL-02-089, Warszawa, Poland

[4]Department of Invertebrate Paleontology, American Museum of Natural History, New York, USA

[5]Department of Earth and Planetary Sciences, Northwestern University, Evanston, IL, USA

[6]Department of Paleobiology, National Museum of Natural History, Smithsonian Institution, Washington, DC, USA

BSS, 0000-0003-3595-5168; BRJ, 0000-0002-1228-515X; NL, 0000-0003-0038-8079; BBS, 0000-0001-5397-6654

*Correspondence: bsinger@wisc.edu

Abstract: Improvements in analytical procedures in parallel with intercalibration of $^{40}Ar/^{39}Ar$ and U–Pb methods and laboratories, spurred since 2003 by the EarthTime geochronology community initiative, have led to $\pm 2\sigma$ uncertainties of the order of 50–100 ka, or better, for Cretaceous ash beds. Assembled here are 57 $^{40}Ar/^{39}Ar$ ages and 17 ^{238}U–^{206}Pb ages of volcanic ash beds in strata of the Western Interior Basin of North America determined during the last 15 years since these improvements have been made. These age determinations span from 108 Ma in the middle Albian to 66 Ma in the latest Maastrichtian. Five of the $^{40}Ar/^{39}Ar$ ages from Campanian and Maastrichtian strata are newly reported here, whereas the remainder are from the literature. Building on the pioneering work of John Obradovich and Bill Cobban, where possible these age determinations are tied to ammonite and inoceramid biostratigraphy. For most ash beds, the temporal uncertainties, unlike earlier timescales for the Western Interior Basin, are much shorter than the duration of fossil biozones. Proposed ages for stage boundaries based on this review of the radioisotopic ages include: Maastrichtian–Danian, 66.02 ± 0.08 Ma; Campanian–Maastrichtian, 72.20 ± 0.20 Ma; Santonian–Campanian, 84.19 ± 0.38 Ma; Coniacian–Santonian, 86.49 ± 0.44 Ma; Turonian–Coniacian, 89.75 ± 0.38 Ma; Cenomanian–Turonian, 93.95 ± 0.05 Ma; Albian–Cenomanian, 100.00 ± 0.40 Ma.

Six bentonites that occur within the *Vascoceras diartianum, Neocardioceras juddi, Prionocylus macombi, Scaphites preventricosus, Scaphites depressus* and *Desmoscaphites bassleri* ammonite zones, dated using both $^{40}Ar/^{39}Ar$ and U–Pb methods, yield ages in agreement to within 150 ka and form the backbone of the Western Interior Basin timescale. In parallel, improvements in the taxonomy of ammonites, inoceramids and foraminifera, and recent field work, are better establishing the biostratigraphic framework for these age determinations. Each of these efforts contributes to the progressive refinement of the chronostratigraphic framework of the Western Interior Basin, and enhances its utility for global correlation.

Supplementary material: An updated zonal chart, summary of age determinations, complete argon isotope data from seven samples and a KMZ file for import into Google Earth are available at https://doi.org/10.6084/m9.figshare.c.6895395

Geochronological background

The Western Interior Basin of North America (Fig. 1; for overview, see Miall *et al.* 2008) has played a critical role in establishing a timescale for the Cretaceous period owing to the pioneering work of Obradovich and Cobban (1975), Obradovich (1993), Hicks *et al.* (1999, 2002) and Cobban *et al.* (2006), who integrated the provincial and global biostratigraphy of molluscan fauna with generations of ever-improving radioisotopic age determinations. An initial timescale capitalized on conventional

From: Hart, M. B., Batenburg, S. J., Huber, B. T., Price, G. D., Thibault, N., Wagreich, M. and Walaszczyk, I. (eds) 2025. *Cretaceous Project 200 Volume 1: the Cretaceous World*. Geological Society, London, Special Publications, **544**, 367–391. First published online December 5, 2023, https://doi.org/10.1144/SP544-2023-76

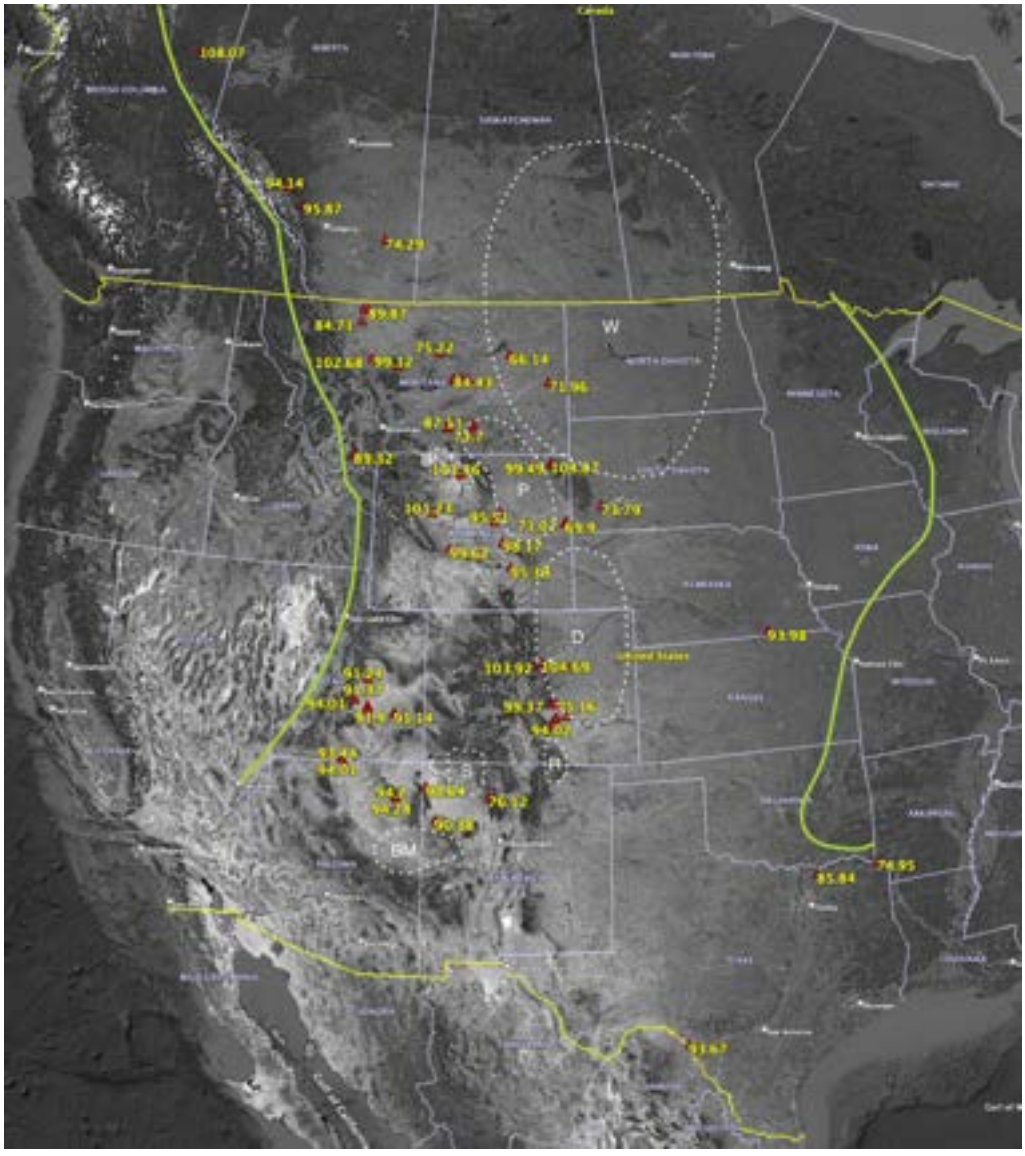

Fig. 1. Locations of dated bentonite samples (red triangles) with ages in Ma (yellow) from within the Western Interior Basin (Table 1). Green lines approximate the western and eastern boundaries of the Western Interior Basin during its greatest (Early Turonian) extent (from Miall *et al.* 2008). White dashed lines approximate limits of Maastrichtian–Eocene basins including Williston (W), P (Powder River), B (Bighorn), D (Denver), R (Raton), S (San Juan) and BM (Black Mesa). Table S4_Age_ID_KMZ.csv in the Supplementary Material contains these locations, ages and uncertainties, and can be imported into Google Earth. Source: base map from Google Earth.

K–Ar age determinations from biotite and sanidine crystals separated from 17 bentonitic ash beds associated with 15 faunal zones from the Albian *Neogastroplites cornutus* Zone at *c.* 95 Ma to *Triceratops* at 64–66 Ma (Obradovich and Cobban 1975). Nearly two decades later, Obradovich (1993) utilized hand-picked separates of sanidine feldspar from 32 bentonitic ash beds to greatly expand this timescale and improved its accuracy and precision by taking advantage of the $^{40}Ar/^{39}Ar$ variant of K–Ar dating. The ages determined by Obradovich (1993) span from the lowermost Albian in Germany at 114.0 $\pm$ 1.30 Ma ($\pm 2\sigma$ analytical uncertainty) to the lower Z coal in the basal Paleogene Fort Union Formation

near Hell Creek, Montana at 65.35 ± 0.31 Ma. These $^{40}Ar/^{39}Ar$ ages are associated with 29 faunal zones of mainly ammonites and are calibrated relative to sanidine from the Taylor Creek rhyolite with an age of 28.32 Ma, similar to an age of 28.02 Ma for the widely used Fish Canyon sanidine standard. Focusing on the Campanian and Maastrichtian succession at Red Bird, Wyoming, in which a detailed ammonite biostratigraphy is established (Gill and Cobban 1966), Hicks *et al.* (1999) – using methods of Obradovich (1993) – determined the $^{40}Ar/^{39}Ar$ ages of seven Western Interior Basin bentonitic ash beds between 81 and 69 Ma that also constrain the timing of geomagnetic polarity chron boundaries including the C32n/C31r at 70.44 ± 0.7 Ma and C31r/C31n at 69.01 ± 0.5 Ma. The development of an Upper Cretaceous Western Interior Basin timescale propelled by the $^{40}Ar/^{39}Ar$ ages determined by John Obradovich at laboratories of the US Geological Survey culminated with the publication in 2006 of a zonal table of Cenomanian–Maastrichtian ammonites and inoceramids with corresponding $^{49}Ar/^{39}Ar$ ages (Cobban *et al.* 2006).

Advances in radioisotopic dating

Since the publication of the Cobban *et al.* (2006) zonal table, geochronology community efforts, propelled by the EarthTime initiative (Condon *et al.* 2016) that aimed towards calibrating the Phanerozoic history of life on Earth at permil levels of temporal resolution, have greatly reduced interlaboratory biases, improved the accuracy of the $^{40}Ar/^{39}Ar$ and U–Pb chronometers, and brought these two radioisotopic systems into close agreement (e.g. Kuiper *et al.* 2008; Schmitz and Kuiper 2013). A key advance is the astronomical calibration of the $^{40}Ar/^{39}Ar$ method, which resolved debate about the age of the widely used Fish Canyon sanidine standard mineral. The preferred age of 28.201 ± 0.046 Ma, an increase of 0.65% over earlier values, reduces systematic uncertainties of the method by an order of magnitude (Kuiper *et al.* 2008). The latter standard age has been adopted by Gradstein *et al.* (2012, 2020) in the *Geologic Time Scale* volumes for reasons explained in Schmitz (2012) and Schmitz *et al.* (2020). Further advances in standardization, determination of decay constants and multi-collector mass spectrometry, which have improved the precision and accuracy of both the $^{40}Ar/^{39}Ar$ and U–Pb methods, are reviewed in Schmitz *et al.* (2020), Schaltegger *et al.* (2021) and Schaen *et al.* (2021).

In 2008, John Obradovich and Bill Cobban provided access to their archives of field notes, stratigraphic information, purified sanidine samples and $^{40}Ar/^{39}Ar$ isotopic data in paper form, much of which had not been published. In the WiscAr lab at the University of Wisconsin-Madison, a new set of $^{40}Ar/^{39}Ar$ sanidine ages was determined for many of the key bentonites, but these relied on a type of single-collector mass spectrometer similar to the one used by Obradovich at the USGS Menlo Park lab (Singer *et al.* 2021). A larger number of dates per sample were generated (typically $n = 6$–7 for Obradovich, v. $n = 30$–40 at WiscAr lab). The $^{40}Ar/^{39}Ar$ ages were cross-calibrated against single-zircon U–Pb ages determined by chemical abrasion isotope-dilution thermal ionization mass spectrometry (CA-IDTIMS) at the British Geological Survey in Keyworth, UK from bentonites at the same localities collected by Cobban and analysed by Obradovich (1993). The results were used to integrate for the first time $^{40}Ar/^{39}Ar$, U–Pb and astronomical clocks, and thus establish age models that span 12 Myr from the Cenomanian through the Lower Campanian (Meyers *et al.* 2012; Sageman *et al.* 2014). This effort reveals that the U–Pb zircon and $^{40}Ar/^{39}Ar$ sanidine dates are brought into close agreement by using the Kuiper *et al.* (2008) age of 28.201 ± 0.046 Ma for the Fish Canyon sanidine standard, thereby strongly supporting the astronomical calibration of the method. Using a carbon and oxygen-isotope chemostratigraphy (Joo and Sageman 2014), together with these $^{40}Ar/^{39}Ar$ and U–Pb ages and independent astrochronological age models, Sageman *et al.* (2014) proposed new ages for the Turonian–Coniacian, Coniacian–Santonian and Santonian–Campanian stage boundaries (Fig. 2).

Multi-collector mass spectrometers have more stable electronics (e.g. Schaen *et al.* 2021), which result in $^{40}Ar/^{39}Ar$ dates for single Cretaceous sanidine crystals with analytical uncertainties of less than ± 100 ka. In the WiscAr lab, a Noblesse multi-collector mass spectrometer is fitted with four ion counting electron multipliers that can produce $^{40}Ar/^{39}Ar$ dates with a significant improvement in precision compared with those obtained using a single-collector mass spectrometer (Jicha *et al.* 2016). Thus, a small population of dates can have resulting weighted mean depositional ages with analytical uncertainties of ± 30 to 50 kyr, i.e. better than 0.5 permil. Thus, the multi-collector mass spectrometer is poised to improve the precision and accuracy of the legacy data in Obradovich (1993) and Hicks *et al.* (1999, 2002) by nearly an order of magnitude.

As an example that highlights both the advantages and challenges of improved precision, Jones *et al.* (2021) determined ages from three bentonites at Nipple Creek, Utah, which are thought to be equivalent to widespread marker bentonites B, C and D of Elder (1988) that bracket the Cenomanian–Turonian boundary and help to define the duration of ocean anoxic event 2 (Fig. 3). Incremental heating of individual sanidine crystals from the three Nipple Creek bentonites B, C and D yield

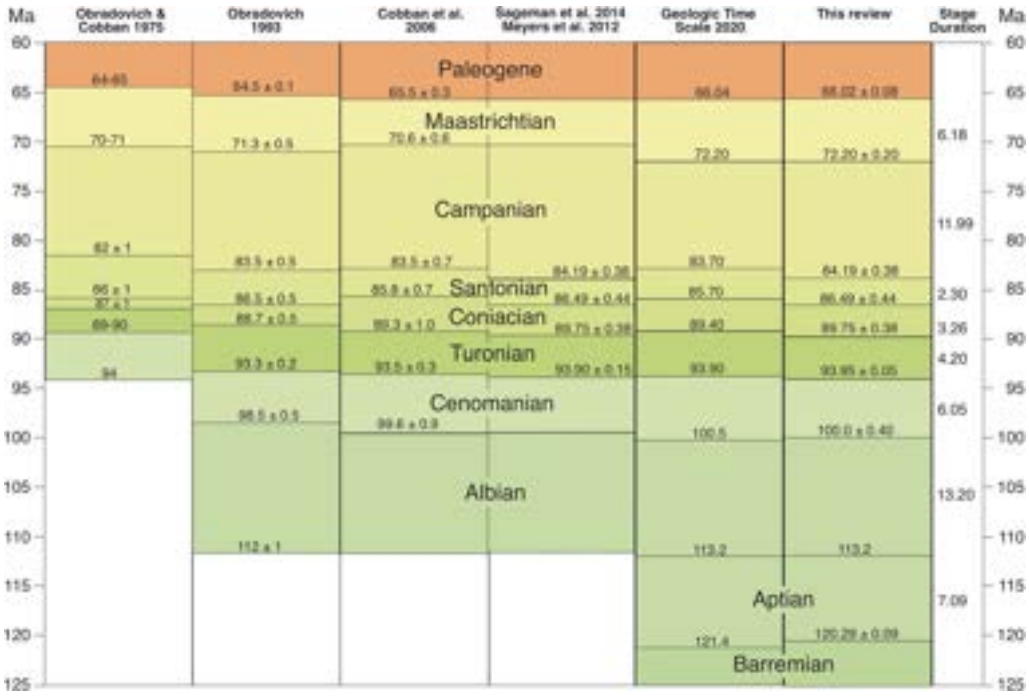

Fig. 2. Evolution of stage boundary ages in successive timescales derived mainly from dating bentonites in the Western Interior Basin. Geological Time Scale 2020 is from Gradstein *et al.* (2020). Stage durations in Myr are estimates based on this review. The inferred age of the Barremian–Aptian stage boundary of 120.29 ± 0.09 Ma is from Li *et al.* (2023).

ages of 94.082 ± 0.057, 94.011 ± 0.060 and 93.443 ± 0.090 Ma, respectively (±2σ uncertainties including contributions from the *J*-value; Jones *et al.* 2021). Moreover, Jones *et al.* (2021) determined single-crystal fusion ages from two bentonite samples in the *Watinoceras devonense* Ammonite Zone, K-07-01-C from the Cenomanian–Turonian Global Stratotype Section and Point (GSSP) at Pueblo, Colorado, and Obradovich sample 90-O-34 from Lohali Point, Arizona, in part to address dispersion of a few U–Pb and $^{40}Ar/^{39}Ar$ dates in Meyers *et al.* (2012). The results from experiments on the Elder (1988) B and C correlative bentonites, together with a U–Pb zircon age of 94.14 ± 0.12 Ma of a B bentonite correlative in Alberta (Barker *et al.* 2011), yield a Cenomanian–Turonian boundary age of 93.95 ± 0.05 Ma (Fig. 3; Jones *et al.* 2021). Note that the precision of the age determinations in Jones *et al.* (2021) reveals that the U–Pb zircon ages proposed for three B bentonite correlatives in Texas, Colorado and Canada are compromised, likely reflecting pervasive inheritance of older crystals (Fig. 3). This Cenomanian–Turonian boundary example serves to highlight that dispersion of dates in both U–Pb and $^{40}Ar/^{39}Ar$ data sets is common and requires new interpretive strategies to determine depositional ages (e.g. Schaen *et al.* 2021). More recently, Singer *et al.* (2021) determined $^{40}Ar/^{39}Ar$ single sanidine fusion ages from 14 bentonites lower in the Western Interior Basin succession spanning from the Albian Thermopolis shale at 106.37 ± 0.11 Ma to the Cenomanian Mowry shale at 97.52 ± 0.09 Ma.

Advances in the $^{40}Ar/^{39}Ar$ sanidine and U–Pb zircon chronometers have also led to more precise constraints on the timing of the Maastrichtian–Danian boundary and the base of the Paleogene in the Hell Creek and Tullock formations, Montana (Sprain *et al.* 2018) and in the Denver Basin, Colorado (Clyde *et al.* 2016). The U–Pb ages of Clyde *et al.* (2016) suggest a Cretaceous–Paleogene boundary age of 66.02 ± 0.08 Ma that is consistent with the age of 65.85 ± 0.11 Ma inferred from $^{40}Ar/^{39}Ar$ dating by Sprain *et al.* (2018), as well as the $^{40}Ar/^{39}Ar$ age of Chicxulub tektites of 66.038 ± 0.098 Ma (Renne *et al.* 2013) when the total uncertainties of these methods are considered.

The aims of this contribution are threefold: (1) to combine recent $^{40}Ar/^{39}Ar$ and U–Pb age determinations with those from recent literature into a tabular

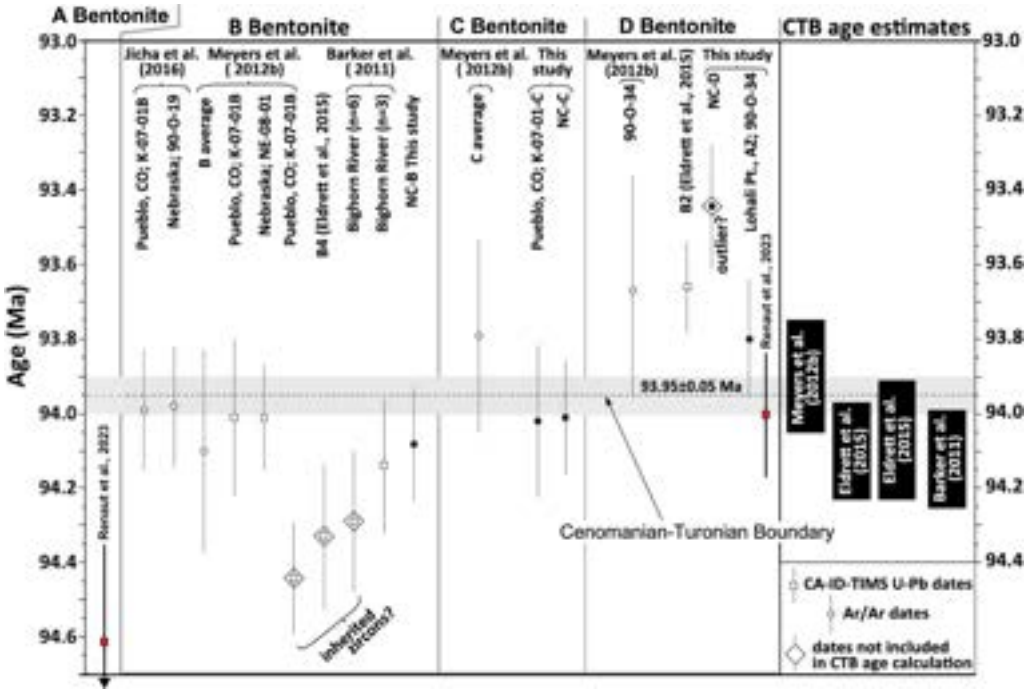

Fig. 3. U–Pb zircon and $^{40}Ar/^{39}Ar$ age determinations that bear on timing of the Cenomanian–Turonian boundary (CTB) which are presented and discussed in the main text. The CTB is between bentonites B and C at the various sections from which ages have been determined. Jones *et al.* (2021) propose a CTB age of 93.95 $\pm$ 0.05 Ma that is compared to other estimates in the right panel. Inherited zircon crystals likely result in weighted mean U–Pb ages that are spuriously old for the B bentonite in three different sections ranging from Texas to Canada. Source: modified from Jones *et al.* (2021).

framework with associated location maps and to provide a summary; (2) to present new $^{40}Ar/^{39}Ar$ single sanidine laser fusion age determinations from four bentonites in Campanian and Maastrichtian strata for which Bill Cobban and John Obradovich provided stratigraphic information and sanidine separates; and (3) to refine, where possible, the correlations of the dated bentonite beds within ammonite and inoceramid faunal zones.

Biostratigraphic overview

Ammonite zonation

The ammonite zonation of the Upper Cretaceous of the Western Interior Basin was first summarized by Cobban and Reeside (1952). Since then, it has undergone many revisions (e.g. Robinson *et al.* 1959; Scott and Cobban 1965, 1975, 1986*a*, *b*; Gill and Cobban 1966; Cobban 1958*a*, *b*; Cobban and Hook 1979; Kennedy and Cobban 1991; Landman and Waage 1993; Kennedy *et al.* 2001), culminating in one of the most refined zonal schemes of any system in the geological record (Cobban *et al.* 2006). Ammonites form the basis of this zonation because they fulfil the essential criteria for index fossils in that they evolved rapidly, producing a series of short-lived species with complex and distinctive morphologies. Within rocks of the Western Interior Basin, these fossils are abundant, facies independent and well preserved.

The taxonomic composition of the ammonites comprising the zonation varies over time. In the Cenomanian and Turonian, most species, such as *Collignoniceras woollgari*, belong to the suborder Ammonitina, and are cosmopolitan in distribution. In the Campanian and Maastrichtian, most species, such as *Baculites clinolobatus*, belong to the Ancyloceratina, and are endemic. The geographical distribution of particular species was influenced by sea-level fluctuations and possible connections with other basins. This affects, in turn, the usefulness for correlating from basin to basin.

The zonal scheme for ammonites is always evolving. As a result of taxonomic revisions, the upper and lower boundaries of some zones have changed and new zones have been added, leading to a more refined zonation. For example, in an early version

of the zonation (Cobban and Reeside 1952), the *Baculites compressus* Zone occupied a thick stratigraphic interval. This species is characterized by an elliptical cross-section, smooth to weakly ribbed venter, and lack of ornament on the flanks, except in large specimens. In subsequent years, Gill and Cobban (1966) recognized the new species *Baculites cuneatus*. This species was previously included in *B. compressus*, but differs from it in having a trigonal cross-section with a very narrow venter, and moderately strong ribbing on the venter and flanks in both small and large specimens. As a consequence of these taxonomic revisions, later versions of the zonation (e.g. Gill and Cobban 1966; Scott and Cobban 1986*a*) include a thinner *B. compressus* Zone overlain by the *B. cuneatus* zone.

Further refinement of the faunal zonation within rocks of the Western Interior Basin has involved the inclusion of additional ammonites, as well as other molluscs, notably inoceramids. For example, the ranges of the co-occurring species of *Hoploscaphites* help anchor the zonation and provide additional means to refine it. For example, *Hoploscaphites plenus*, *H. crassus* and *H. peterseni* are present in the lower part of the *Baculites baculus* Zone whereas *H. macer*, *H. sargklofak* and *H. criptonodosus* are present in the upper part of the *B. baculus* Zone, thus helping to subdivide the zone and support the subdivision suggested by inoceramids.

Radioisotopic age determinations provide estimates of the duration of the ammonite zones and, thus, the geological longevity of ammonite species. Dividing the total time interval by the number of zones yields an estimate of ~450 kyr per zone. However, it is important to note that this is only an average, and the time interval represented by any particular zone varies widely. For example, the durations of some of the ammonite zones in the upper Cenomanian are very short (30–70 kyr) whereas the durations of some of the ammonite zones in the lower Maastrichtian are much longer, ranging from 0.8 to 1.0 Myr. In addition, radioisotopic ages are critical in using modern phylogenetic approaches such as Bayesian tip dating, allowing the most effective means to reconstruct the phylogeny of various clades. The present zonal scheme consists of 66 ammonite zones stacked one on top of another (Cobban *et al.* 2006).

Inoceramid zonation

Inoceramid bivalves appeared in the Cretaceous of the Western Interior in usable levels of diversity and stratigraphic frequency in the late Albian. Their comparatively abundant presence (dominating many molluscan assemblages, especially in offshore facies) continued in the basin until the final retreat of the sea in the late Maastrichtian. Although inoceramids are inferior to ammonites with respect to their potential to refine regional stratigraphic resolution of Western Interior biozonations (at least in most of the Upper Cretaceous series), they clearly surpass them in terms of potential for inter-regional chronostratigraphic correlation. With the exception of the upper Albian–middle Cenomanian and the middle–lower upper Turonian, the two intervals with very high levels of inoceramid endemism, the group was represented by geographically widespread lineages that were inter-regional to pandemic/cosmopolitan in extent, providing a foundation for direct correlation to regions far outside the Western Interior.

The first evaluation of the stratigraphic potential of inoceramids of the Western Interior Basin was summarized by Cobban and Reeside (1952) – see also discussion in Seitz (1956) – but a complete inoceramid-based biostratigraphic zonation scheme was not proposed until later. Kauffman *et al.* (1978) worked out a detailed zonation for the Cenomanian through Coniacian, and Kauffman *et al.* (1993) did the same for the entire Albian–Upper Cretaceous succession (see also Kauffman 1975). In the late 1990s, the stage-by-stage revision of inoceramid biostratigraphy was started by Cobban and Walaszczyk and published in a series of subsequent papers (Walaszczyk and Cobban 2000, 2006, 2007, 2016; Walaszczyk *et al.* 2001). The summary chart for the year 2006 was published by Cobban *et al.* (2006) with numerous subsequent modifications; its most recent 2023 iteration is shown in Table S1 in the Supplementary Material.

Since the formulation of the classic Upper Cretaceous stage definitions, primarily on the basis of orthostratigraphic ammonites (e.g. Hancock 1984), inoceramids have gradually gained in importance. The bases of two of these stages, the Coniacian and Santonian, are in fact defined with inoceramids, and the group serves as a good proxy for the Cenomanian, Turonian and Maastrichtian stage boundaries. The group's potential for substage level definitions of Upper Cretaceous stages is at least as high. Using inoceramids, several of the radioisotopic ages from the Western Interior Basin succession may be directly transferred or extrapolated on to stage/substage boundaries. Moreover, precise radioisotopic ages allow for quantifying the rate of evolutionary and biogeographical processes which led to the observed palaeontological record and are thus important to understanding its stratigraphic value.

Methods

$^{40}Ar/^{39}Ar$ analysis in the WiscAr Lab

Six of the seven sanidine separates from which new $^{40}Ar/^{39}Ar$ data are obtained were provided by John

Obradovich, including samples 92-O-13, 86-O-05, 92-O-31, 91-O-12, 92-O-32 and 91-O-09. One sample, WY-10-03, was collected by Singer from bed #112 in the Red Bird, Wyoming section of Gill and Cobban (1966). The stratigraphic context, biostratigraphic position and location for each of these samples are summarized in Table 1. From the vials of separates provided by Obradovich, sanidine crystals were identified using a variable pressure scanning electron microscope. From bentonite sample WY-10-03, sanidine was isolated using magnetic and gravity separation, and identified using a variable pressure scanning electron microscope (methods summarized in Sageman *et al.* 2014). Sanidine separates were ultrasonically leached in 1.5 M HF for several minutes and rinsed repeatedly with deionized water prior to SEM identification. The seven sanidine separates were wrapped in aluminium foil, placed in one of 17 wells, each 4 mm in diameter by 4 mm deep, in an aluminium disk that is 2.5 cm in diameter. Several crystals of the 28.201 ± 0.046 Ma Fish Canyon sanidine standard (Kuiper *et al.* 2008) were placed with the samples in each well. Irradiations were for 50 hours in the cadmium-lined inner-core irradiation tube of the Oregon State University TRIGA reactor. *J*-values for each sample are based on single crystal analyses of 8–12 Fish Canyon sanidine monitors in each well of the irradiation disk. No interpolation or modelling of *J*-values is attempted because samples and monitor crystals were co-located in the same well.

Single crystal fusion experiments in the WiscAr laboratory at the University of Wisconsin-Madison were undertaken with a 50 W CO_2 laser, followed by gas analysis in a Noblesse multi-collector mass spectrometer, as in Jicha *et al.* (2016). For two samples, 92-O-13 from a 15 cm thick bentonite in the Lewis Shale in New Mexico (Hicks *et al.* 1999) and 86-O-05 from the Annona Formation in Arkansas (Obradovich 1993), single-collector mass spectrometry as in Sageman *et al.* (2014) was used and these samples were irradiated for 60 and 90 hours, respectively.

The isotopic composition of atmospheric argon used to calculate radiogenic argon percentages is from Lee *et al.* (2006). Ages are calculated using the decay constants of Min *et al.* (2000), and are reported as $\pm X/Y/Z$, where X is the internal analytical uncertainty at the 95% confidence level, Y is this internal uncertainty, plus that contributed by measurement of the *J*-value, and Z is the total uncertainty, which includes the internal and *J*-value uncertainties, plus systematic contributions from uncertainty in the ^{40}K decay constant and age of the Fish Canyon sanidine standard. The total uncertainties are calculated using the ArAR software program (Mercer and Hodges 2016) and this resulted in changes for ages originally reported by Sageman *et al.* (2014). Note that for a small number of the age determinations discussed below, either the analytical uncertainty (X) or the tracer uncertainty (Y) is not published, and hence the uncertainties are discussed as they are listed in Table 1.

Radioisotopic database representing the Cretaceous Western Interior Basin

Table 1 summarizes 74 radioisotopic age determinations from bentonitic ash beds deposited primarily in marine sediment sequences (available as an excel spreadsheet in Table S2 of the Supplementary Material). It is beyond the scope of our effort to include and review the expansive set of age determinations from continental sediments deposited along the margins of the Western Interior Seaway that are used to evaluate the tempo of terrestrial vertebrate evolution (e.g. Ramezani *et al.* 2022). Of these 74 age determinations, 17 are based on CA-IDTIMS U–Pb single zircon dating results found in: Barker *et al.* (2011), Meyers *et al.* (2012), Sageman *et al.* (2014), Eldrett *et al.* (2015), Clyde *et al.* (2016), Ramezani *et al.* (2022) and Renaut *et al.* (2023). Fifty-two of the age determinations in Table 1 are from $^{40}Ar/^{39}Ar$ results found in: Oboh-Ikuenobe *et al.* (2008), Siewert (2011), Meyers *et al.* (2012), Zhu *et al.* (2012), Sageman *et al.* (2014), Ma *et al.* (2014), Jicha *et al.* (2016), Landman *et al.* (2018, 2020), Sprain *et al.* (2018), Lin *et al.* (2021), Jones *et al.* (2021), Kynaston *et al.* (2021) and Singer *et al.* (2021). Five additional $^{40}Ar/^{39}Ar$ age determinations in Table 2 are reported in the results section. Where possible, United States Geological Survey Denver 'D' numbers linked to digital records of ammonite or inoceramid fossil localities (McKinney 2018) are listed in Table 1 to provide the biostratigraphic context of the dated bentonitic ash layers. A more comprehensive zonal chart of radioisotopic age determinations, to which we have added ages based on legacy data in Obradovich (1993) for samples yet to be dated using modern multi-collector mass spectrometry, is provided in the Supplementary Material.

Results

$^{40}Ar/^{39}Ar$ data from experiments on samples from seven bentonites in the WiscAr laboratory are summarized in Table 1 and Figure 4. Complete isotopic data are provided in Table S3 of the Supplementary Material. Samples 92-O-13, 86-O-05, 92-O-32, WY-10-03 and 91-O-09 yield distributions of sanidine dates that give ages which are consistent with their biostratigraphic position. In contrast, samples 92-O-31 and 91-O-12 yield dates that are significantly older than expected based on the positions

Table 1. Summary of Western Interior Basin tuffs in marine sediments dated by single sandine $^{40}Ar/^{39}Ar$ and single zircon CA-IDTIMS U–Pb methods

Sample	Source	USGS D number	Stratigraphic description	Inoceramid Zone	Ammonite Zone
HF-1PR	16		Ash bed base Paleogene, Tulloch Formation (six samples)		
Maastrichtian–Danian boundary 66.02 ± 0.08 Ma (Clyde *et al.* 2016)					
KJ08-157	14		Uppermost Cretaceous, D1 of Denver Formation in Bowring Pit		
Null Coal	16		Uppermost Cretaceous, Hell Creek Formation		
WY-10-03	1	D4349	Base of Fox Hills sandstone, bed #112 of Gill and Cobban (1966)		*Baculites clinolobatus*
92-O-32	1	D2118	1.4 m bentonite bed #97 in Pierre Shale of Gill and Cobban (1966)		*Baculites grandis*
2807	13		Pierre Shale	*Inoceramus incurvus*	*Baculites baculus*
Campanian–Maastrichtian boundary 72.20 ± 0.20 Ma (Gradstein *et al.* 2020)					
92-O-34	13		Pierre Shale	*Inoceramus redbirdensus*	*Baculites eliasi*
90-O-15	12	D13111	22 cm bentonite #3, 1.5 m above base of compressus zone in Bearpaw Shale	*Inoceramus altus*	*Baculites compressus*
3504	12		Pierre Shale, associated with methane seep		*Baculites compressus*
IL082717-1	17		Bearpaw tuff, Bearpaw Shale		
93-O-16	11	D13437 D13438	Pierre Shale	*Sphaeroceramus pertenuiformis*	*Exiteloceras jenneyi*
86-O-05	1		20 cm bentonite, Anonna Formation, 5 m above lowest occurrence of *G. calcarata*		
90-O-54	12	D12704	Pierre Shale		*Didymoceras stevensoni*
PPF1-03	17		PPF tuff		
92-O-13	1		15 cm bentonite in Lewis Shale (Hicks *et al.* 1999)		*Baculites scotti*
78-O-05	3	D5636	Telegraph Creek Formation	*Sphenoceramus* cf. *lingua*	*Scaphites hippocrepis II*
Santonian–Campanian 84.19 ± 0.38 Ma (Sageman *et al.* 2014)					
MT-08-04	3		Same as Obradovich (1993) sample 68-O-04		*Demoscaphites bassleri*
MT-08-04	3		Same as Obradovich (1993) sample 68-O-04		*Demoscaphites bassleri*
91-O-09	3		Bentonite in Kevin Member, Marias River Formation		*Demoscaphites erdmanni*
90-O-10	3		10 cm bentonite 16 m below top of Cody Shale		*Clioscaphities vermiformis*
92-O-14	3		Austin Chalk	*Cladoceramus undulatoplicatus*	
Coniacian–Santonian 86.49 ± 0.44 Ma (Sageman *et al.* 2014)					
MT-11-03	3		Kevin Member, Telegraph Creek Formation	*Sphenoceramus subcardissoides*	*Scaphites depressus*
91-O-08	3	D13200	Cody Shale, 30.5 m above top of Kevin bentonite group		*Scaphites depressus* = *Protexanites bourgeoisianus*
MT-08-01	3		Same as Obradovich sample 91-O-8		*Scaphites depressus* = *Protexanites bourgeoisianus*
UH-BHA-B5	19		15–20 cm bentonite, ~2.5 m above Ferron SS-Blue Gate shale contact		
91-O-13	3		Marias River Shale	*Cremnoceramus deformis crassus*	*Scaphites preventricosus*
MT-08-03	3		Same as Obradovich sample 91-O-13	*Cremnoceramus deformis crassus*	*Scaphites preventricosus*
Turonian–Coniacian 89.75 ± 0.38 Ma (Sageman *et al.* 2014)					
MT-09-09	3		Ferdig Member, bed#39, Marias River Shale		*Scaphites nigricollensis*
PS9	21		Gallup Formation	*Inoceramus perplexus*	*S. whitfieldi*, *P. novimexicanus*
'Lower bentonite'	21		Gallup Formation	*Inoceramus dimidius*	*S. warreni*, *P. wyomingensis*
UH-BHA-B4	20		2 cm bentonite above a coal seam in the Ferron Sandstone		*Scaphites warreni*
FN-BHt	20		Middle of three dated bentonites in mid-upper Ferron Sandstone		*Scaphites warreni*
UH-BHA-B3	20		10–15 cm bentonite in the Ferron Sandstone		*Scaphites warreni*
UT-08-03	3		40 cm thick bentonite, crystal rich lower half. In Mancos Shale		*Prionocylus macombi*
UT-08-03	3		40 cm thick bentonite, crystal rich lower half. In Mancos Shale		*Prionocylus macombi*
UH-BHA-B1	20		Lower bentonite from triplet of bentonites in Tununk Shale		*Prionocylus hyatti*
NC-D	4		Nipple Creek, Utah, Ash D of Elder (1988)		*Vascoceras birchbyi*
B3	8		Shell research core Iona-1, Kinney Co, TX		
90-O-34	4		Likely correlative to C bentonite of Elder (1988)		*Vascoceras birchbyi*
TT4 ash	15		Ash in Tununk Shale		*Vascoceras birchbyi; P. flexuosum*
NC-C	4		Nipple Creek, UT, Ash C of Elder (1988)		*Watinoceras devonense*

Sample	Location	Latitude	Longitude	Elev. (masl)	Method	Age (Ma)	$\pm 2\sigma_{int}$	$\pm 2\sigma_{int+J}$ $\pm 2\sigma_{tr}$	$\pm 2\sigma_{tot}$
HF-1PR	Hell Creek, IRZ hill, MT	47.53544	−107.1734	879	$^{40}Ar/^{39}Ar$	**65.84**	±0.02	±0.02	±0.18
Maastrichtian–Danian boundary 66.02 ± 0.08 Ma (Clyde *et al.* 2016)									
KJ08-157	Denver Basin, Bijou Creek section, CO	39.57059	−104.3031	1413	U–Pb	**66.08**	±0.02	±0.04	±0.08
Null Coal	Hell Creek area, Bug Creek section, MT	47.67630	−106.2101	691	$^{40}Ar/^{39}Ar$	**66.14**	±0.29	±0.30	±0.35
WY-10-03	Redbird, WY USGS section	43.27086	−104.2713	1228	$^{40}Ar/^{39}Ar$	**69.90**	±0.04	±0.09	±0.13
92-O-32	Redbird, WY USGS section	43.27586	−104.2665	1242	$^{40}Ar/^{39}Ar$	**71.02**	±0.05	±0.09	±0.13
2807	Dawson County, MT	46.93742	−104.7345	685	$^{40}Ar/^{39}Ar$	**71.96**	±0.05	±0.08	±0.13
Campanian–Maastrichtian boundary 72.20 ± 0.20 Ma (Gradstein *et al.* 2020)									
92-O-34	Garfield County, MT	47.00603	−107.7725	862	$^{40}Ar/^{39}Ar$	**72.47**	±0.06	±0.07	±0.12
90-O-15	Bighorn County, MT	45.83444	−107.5796	903	$^{40}Ar/^{39}Ar$	**73.70**	±0.12	±0.13	±0.16
3504	Red Shirt Creek, Custer Co., SD	43.69333	−102.9767	895	$^{40}Ar/^{39}Ar$	**73.79**	±0.33	±0.36	±0.38
IL082717-1	Dinosaur Park, Alberta, Canada	50.75583	−111.3811	734	U–Pb	**74.29**	±0.01	±0.02	±0.08
93-O-16	South bank Andy Creek, Pueblo Co., CO	38.32960	−104.4010	1436	$^{40}Ar/^{39}Ar$	**74.67**	±0.10	±0.12	±0.16
86-O-05	Foreman Quarry, Foreman, AR	33.69464	−94.4113	106	$^{40}Ar/^{39}Ar$	**74.95**	±0.08	±0.10	±0.14
90-O-54	East side, Interstate 25, 4 km south of Fountain, CO	38.64743	−104.6949	1681	$^{40}Ar/^{39}Ar$	**75.16**	±0.08	±0.12	±0.16
PPF1-03	Fergus County, MT	47.72478	−108.9435	825	U–Pb	**75.22**	±0.03	±0.05	±0.09
92-O-13	Rio Arriba County, NM	36.23942	−106.9105	2229	$^{40}Ar/^{39}Ar$	**76.12**	±0.07	±0.09	±0.14
78-O-05	Petroleum County, 11 km WNW of Mosby, MT	47.02972	−108.0129	870	$^{40}Ar/^{39}Ar$	**81.84**	±0.07	±0.11	±0.16
Santonian–Campanian 84.19 ± 0.38 Ma (Sageman *et al.* 2014)									
MT-08-04	McDonald Creek, MT	47.00440	−108.3340	897	$^{40}Ar/^{39}Ar$	**84.41**	±0.13	±0.14	±0.18
MT-08-04	McDonald Creek, MT	47.00440	−108.3340	897	U–Pb	**84.43**	±0.09		±0.15
91-O-09	Toole County, West of Shelby, MT	48.49227	−112.0303	1090	$^{40}Ar/^{39}Ar$	**84.71**	±0.05	±0.11	±0.16
90-O-10	Bighorn County, MT	45.72241	−107.5790	923	$^{40}Ar/^{39}Ar$	**85.66**	±0.08	±0.09	±0.15
92-O-14	Grayson Co., TX	33.61498	−96.4405	193	$^{40}Ar/^{39}Ar$	**85.84**	±0.23	±0.24	±0.27
Coniacian–Santonian 86.49 ± 0.44 Ma (Sageman *et al.* 2014)									
MT-11-03	NW of Kevin, MT	48.81720	−112.0015	1122	$^{40}Ar/^{39}Ar$	**86.52**	±0.09	±0.12	±0.17
91-O-08	Yellowstone River, Billings, MT	45.74070	−108.5119	1032	$^{40}Ar/^{39}Ar$	**87.13**	±0.07	±0.09	±0.18
MT-08-01	Yellowstone River, Billings, MT	45.74069	−108.5119	1032	U–Pb	**87.11**	±0.08		±0.15
UH-BHA-B5	Caineville, UT	38.49489	−110.9229	1468	$^{40}Ar/^{39}Ar$	**87.27**	±0.52	±0.54	±0.55
91-O-13	Toole County, MT	44.95650	−111.8921	972	$^{40}Ar/^{39}Ar$	**89.32**	±0.09	±0.11	±0.17
MT-08-03	Toole County, MT	48.42882	−111.8921	972	U–Pb	**89.37**	±0.07		±0.15
Turonian–Coniacian 89.75 ± 0.38 Ma (Sageman *et al.* 2014)									
MT-09-09	Kevin-Sunburst Dome 10 km SE of Sunburst, MT	48.81770	−111.8156	1066	$^{40}Ar/^{39}Ar$	**89.87**	±0.06	±0.10	±0.16
PS9	San Juan Basin, NM	35.60918	−108.6171	2169	$^{40}Ar/^{39}Ar$	**90.38**	±0.12	±0.15	±0.20
'Lower bentonite'	San Juan Basin, NM	36.48273	−108.9212	1962	$^{40}Ar/^{39}Ar$	**90.64**	±0.17	±0.24	±0.27
UH-BHA-B4	Henry Mtns Basin, Wayne County, UT	38.34991	−110.0234	1308	$^{40}Ar/^{39}Ar$	**91.14**	±0.09	±0.19	±0.22
FN-BHt	Henry Mtns Basin, Wayne County, UT	38.36280	−110.9009	1388	$^{40}Ar/^{39}Ar$	**91.15**	±0.11	±0.11	±0.18
UH-BHA-B3	Henry Mtns Basin, Wayne County, UT	38.48192	−110.8794	1399	$^{40}Ar/^{39}Ar$	**91.16**	±0.31	±0.36	±0.38
UT-08-03	Castle Dale Dome, Emery County, UT	39.22256	−110.9486	1752	$^{40}Ar/^{39}Ar$	**91.24**	±0.05	±0.09	±0.23
UT-08-03	Castle Dale Dome area, Emery Co., UT	39.22256	−110.9486	1752	U–Pb	**91.37**	±0.08		±0.15
UH-BHA-B1	Henry Mtns Basin, Wayne County, UT	38.36204	−110.0258	1210	$^{40}Ar/^{39}Ar$	**91.90**	±0.12	±0.12	±0.19
NC-D	Nipple Creek, UT	37.12300	−111.6720	1271	$^{40}Ar/^{39}Ar$	**93.44**	±0.05	±0.09	±0.17
B3	West Texas	29.22517	−100.7415	292	U–Pb	**93.67**	±0.04		±0.12
90-O-34	Lohali Point, AZ	36.18470	−109.8836	2030	$^{40}Ar/^{39}Ar$	**93.80**	±0.05	±0.07	±0.15
TT4 ash	South of Wasatch Plateau, Central UT	38.66513	−111.3447	2022	U–Pb	**94.01**	±0.02	±0.05	±0.11
NC-C	Nipple Creek, UT	37.12300	−111.6720	1271	$^{40}Ar/^{39}Ar$	**94.01**	±0.05	±0.06	±0.15

(*Continued*)

Table 1. *Continued.*

Sample	Source	USGS D number	Stratigraphic description	Inoceramid Zone	Ammonite Zone
K-07-01C	4		Bentonite in Pueblo, CO GSSP, Correlated to Ash C of Elder (1988)	*Mytiloides puebloensis*	*Watinoceras devonense*
Cenomanian–Turonian 93.95 ± 0.05 Ma (Jones *et al.* 2021)					
90-O-19	7		Bentonite in Greenhorn Limestone, bed H-3 of Hattin (1975)		*Neocardioceras juddi*
K-07-01B	7		Bentonite in Pueblo, CO GSSP, Correlated to Ash B of Elder (1988)		*Neocardioceras juddi*
NE-08-01	5		Bentonite in Greenhorn Limestone, bed H-3 of Hattin (1975), same as 90-O-19 site		*Neocardioceras juddi*
NC-B	4		Nipple Creek, Utah, Ash B of Elder (1988)		*Neocardioceras juddi*
Bighorn River	6		Correlated to Ash B of Elder (1988); youngest 3 zircons (Jones *et al.* 2021)		*Neocardioceras juddii*
AZLP-08-02	5		Experiments also on Obradovich (1993) sample 90-O-31/bed BM-15 (Kirkland 1991)		*E. septemseriatum; Scipinoceras gracile*
AZLP-08-01	5		Same as 90-O-30; bed BM-5 (Kirkland 1991)		*Vascoceras diartianum*
TT1 Naturita	14		Ash in Naturita sandstone. Correlated to Ash A of Elder (1988)		*Scipinoceras gracile*
90-O-30	5		Bed BM-5 (Kirkland 1991)		*Vascoceras diartianum*
D2315	11		Frontier Formation	*Inoceramus prefragilis*	*Dunveganoceras pondii*
90-O-50	18		1.6 m thick, Soap Creek (or X) bentonite, Frontier Fm. Same as sample WY-08-04		*Acanthoceras amphibolum*
X bentonite	6		'X' bentonite, Belle Fourche Formation		*Acanthoceras amphibolum?*
91-O-03	10		Thatcher bentonite	*Inoceramus macconnelli*	*Conlinoceras tarrantense*
90-O-51	2		Topmost bentonite, Mowry Shale, near Kaycee		
68-O-09	2		'Clay Spur' bentonite, local top of Mowry Shale		*Neogastropolites americanus*
MT-09-06	2		Arrow Creek bentonite, Colorado Shale,		*Neogastroplites cornutus*
7JDO35	9		Dry Creek Canyon Member, lower upper Dakota Sandstone		
74-O-22	2		Newcastle Sandstone-upper bentonite		
98-O-04	2		Newcastle Sandstone-middle bentonite		
93-O-25	2		Shell Creek Shale, above Muddy Sandstone		
WY-09-08	2		Upper Shell Creek Shale		*Neogastroplites haasi*
97-O-20	2		Shell Creek Shale, basal bentonite, Soap Creek Dome		
Albian–Cenomanian 100.0 ± 0.40 Ma (Singer *et al.* 2021)					
95-O-04	2		Muddy Sandstone, upper of 2 upper bentonites, Maverick Springs		
97-O-01	2		Uppermost Thermopolis Shale just below Muddy Sandstone		
97-O-12	2		2.2–1.5 ft thick water-lain tuff in Mid-Vaughn Member, Blackleaf Fm.		
97-O-13	2		Taft Hill Member bed 27, 48 ft below top of Taft Hill, Blacklead Fm.		
KJ08162	2		Kassler Member, Dakota 'J' Sandstone, No. side Alameda roadcut		
KJ08161	2		Kassler Member, Dakota 'J' Sandstone, So. side Alameda roadcut		
KJ08160	2		Skull Creek Member, Dakota Sandstone, South side roadcut		
93-O-21	2		~4' bentonite, 7 ft above base of Skull Creek Shale		
98-O-08	2		Green marker bentonite, Lower Thermopolis Shale, NW of Greybull		
75-O-06	2		50 m below top Hulcross Fm		*Pseudopulchellia pattoni*

$^{40}Ar/^{39}Ar$ Ages calculated relative to 28.201 Ma Fish Canyon sanidine standard (Kuiper *et al.* 2008) using Min *et al.* (2000) decay constants.
Samples with identification numbers beginning with 68-O, 74-O, 75-O, 90-O, etc. are from John Obradovich.
Data sources: (1) This work, (2) Singer *et al.* (2021), (3) Sageman *et al.* (2014), (4) Jones *et al.* (2021), (5) Meyers *et al.* (2012), (6) Barker *et al.* (2011), (7) Jicha *et al.* (2016), (8) Eldrett *et al.* (2015), (9) Oboh-Ikuenobe *et al.* (2008), (10) Batenburg *et al.* (2016), (11) Ma *et al.* (2014), (12) Landman *et al.* (2018), (13) Landman *et al.* (2020), (14) Clyde *et al.* (2016), (15) Renaut *et al.* (2023), (16) Sprain *et al.* (2018), (17) Ramezani *et al.* (2022), (18) Siewert (2011), (19) Zhu *et al.* (2012), (20) Kynaston *et al.* (2021), (21) Lin *et al.* (2021).
$\pm 2\sigma_{int}$ denotes analytical uncertainty only at the 95% confidence interval.
$\pm 2\sigma_{int+J}$ denotes analytical uncertainty at the 95% confidence interval including *J* uncertainty for $^{40}Ar/^{39}Ar$ ages.
$\pm 2\sigma_{tr}$ denotes analytical plus tracer uncertainty for U–Pb ages.
$\pm 2\sigma_{tot}$ denotes fully propagated uncertainty at the 95% confidence interval including analytical, tracer/standard age and decay constant uncertainties.

Sample	Location	Latitude	Longitude	Elev. (masl)	Method	Age (Ma)	$\pm 2\sigma_{int}$	$\pm 2\sigma_{int+J}$ $\pm 2\sigma_{tr}$	$\pm 2\sigma_{tot}$
K-07-01C	Lake Pueblo State Park, CO	38.28000	−104.7400	1522	$^{40}Ar/^{39}Ar$	**94.02**	±0.14	±0.15	±0.20
Cenomanian–Turonian 93.95 ± 0.05 Ma (Jones *et al.* 2021)									
90-O-19	Thayer County, Nebraska	40.17303	−97.4463	431	$^{40}Ar/^{39}Ar$	**93.98**	±0.03	±0.06	±0.15
K-07-01B	Lake Pueblo State Park, CO	38.28000	−104.7400	1519	$^{40}Ar/^{39}Ar$	**93.99**	±0.03	±0.06	±0.15
NE-08-01	Thayer County, Nebraska	40.17303	−97.4463	431	U-Pb	**94.01**	±0.04		±0.14
NC-B	Nipple Creek, UT	37.12300	−111.6720	1271	$^{40}Ar/^{39}Ar$	**94.08**	±0.03	±0.06	±0.15
Bighorn River	Ram Falls, Ram River, Alberta, CA	52.08756	−115.8429	1614	U–Pb	**94.14**	±0.12		±0.19
AZLP-08-02	Lohali Point, AZ	36.18471	−109.8836	2022	$^{40}Ar/^{39}Ar$	**94.20**	±0.11	±0.15	±0.21
AZLP-08-01	Lohali Point, AZ	36.18471	−109.8836	2021	U–Pb	**94.28**	±0.08		±0.15
TT1 Naturita	South of Wasatch Plateau, Central UT	38.66515	−111.3447	2000	U–Pb	**94.62**	±0.03	±0.05	±0.12
90-O-30	Lohali Point, AZ	36.18471	−109.8836	2021	$^{40}Ar/^{39}Ar$	**94.43**	±0.13	±0.17	±0.22
D2315	Carbon Co., WY	42.13300	−106.2040	2101	$^{40}Ar/^{39}Ar$	**95.39**	±0.16	±0.18	±0.23
90-O-50	Natrona County, WY	43.3108	−106.7776	1696	$^{40}Ar/^{39}Ar$	**95.51**	±0.11	±0.15	±0.26
X bentonite	Burnt Timber Creek, Alberta, CA	51.62897	−115.0408	1359	U–Pb	**95.87**	±0.10	±0.20	±0.30
91-O-03	Pueblo, CO	38.12202	−104.8643	1682	$^{40}Ar/^{39}Ar$	**96.21**	±0.12	±0.16	±0.22
90-O-51	Johnson County, WY	43.57196	−106.5800	1492	$^{40}Ar/^{39}Ar$	**97.52**	±0.04	±0.09	±0.17
68-O-09	Natrona County, WY	42.76562	−106.4728	1684	$^{40}Ar/^{39}Ar$	**98.17**	±0.07	±0.08	±0.16
MT-09-06	Judith Basin County, MT	47.31464	−110.4857	1233	$^{40}Ar/^{39}Ar$	**99.12**	±0.10	±0.14	±0.21
7JDO35	Deadman Canyon, El Paso Cnty, CO	38.67285	−104.8550	1917	$^{40}Ar/^{39}Ar$	**99.37**		±0.31	±0.35
74-O-22	Crook County, WY	44.79557	−104.6586	1327	$^{40}Ar/^{39}Ar$	**99.49**	±0.03	±0.07	±0.17
98-O-04	Crook County, WY	44.79157	−104.6698	1352	$^{40}Ar/^{39}Ar$	**99.58**	±0.03	±0.12	±0.19
93-O-25	SE of Lander, US 287, Fremont County, WY	42.61224	−108.3225	1855	$^{40}Ar/^{39}Ar$	**99.62**	±0.03	±0.07	±0.17
WY-09-08	NE of Greybull, Big Horn County, WY	44.55326	−107.9918	1290	$^{40}Ar/^{39}Ar$	**99.67**	±0.11	±0.13	±0.20
97-O-20	Crow Reservation, Big Horn County, MT	45.26738	−107.7588	1116	$^{40}Ar/^{39}Ar$	**100.07**	±0.03	±0.07	±0.17
Albian–Cenomanian 100.0 ± 0.40 Ma (Singer *et al.* 2021)									
95-O-04	Dome, Fremont County, WY	43.51363	−108.9618	2022	$^{40}Ar/^{39}Ar$	**101.23**	±0.05	±0.09	±0.18
97-O-01	Greybull, Big Horn County, WY	44.52660	−108.0036	1200	$^{40}Ar/^{39}Ar$	**101.36**	±0.05	±0.11	±0.19
97-O-12	So. of Vaughn, Cascade Cnty, MT	47.49533	−111.5302	1124	$^{40}Ar/^{39}Ar$	**102.68**	±0.03	±0.07	±0.18
97-O-13	So. of Vaughn, Cascade Cnty, MT	47.50114	−111.5303	1099	$^{40}Ar/^{39}Ar$	**103.08**	±0.03	±0.11	±0.20
KJ08162	Dinosaur Ridge, Jefferson Cnty, CO	39.67582	−105.1925	1883	U–Pb	**103.92**	±0.04	±0.06	±0.13
KJ08161	Dinosaur Ridge, Jefferson Cnty, CO	39.67563	−105.1926	1884	U–Pb	**104.02**	±0.04	±0.06	±0.13
KJ08160	Dinosaur Ridge, Jefferson Cnty, CO	39.67578	−105.1931	1882	U–Pb	**104.69**	±0.05	±0.07	±0.13
93-O-21	Devils Tower, Crook County, WY	44.81882	−104.7414	1169	$^{40}Ar/^{39}Ar$	**104.87**	±0.04	±0.10	±0.19
98-O-08	Big Horn County, WY	44.57564	−108.1353	1186	$^{40}Ar/^{39}Ar$	**106.37**	±0.04	±0.11	±0.20
75-O-06	Hudson's Hope, BC, Canada	56.10752	−121.8179	607	$^{40}Ar/^{39}Ar$	**108.07**	±0.05	±0.10	±0.20

Table 2. Summary of single sanidine $^{40}Ar/^{39}Ar$ age determinations

Sample	Biozone	*N*	MSWD	Age (Ma)	$\pm 2\sigma_{an}$	$\pm 2\sigma_{int}$	$\pm 2\sigma_{ext}$
WY-10-03	*Baculites clinolobatus*	32/34	0.98	69.90	±0.04	±0.09	±0.13
92-O-32	*Baculites grandis*	29/33	1.03	71.02	±0.05	±0.09	±0.13
91-O-12	*Baculites reesidei*	0/37		Dispersion precludes age determination			
92-O-31	*Didymoceras cheyennense*	0/38		Dates older than biostratigraphic age			
86-O-05	*Radotruncana calcarata*	21/21	0.79	74.95	±0.08	±0.10	±0.14
92-O-13	*Baculites scotti*	27/27	0.57	76.12	±0.07	±0.09	±0.14
91-O-09	*Demoscaphites erdmanni*	31/34	1.19	84.71	±0.05	±0.11	±0.16

Ages calculated relative to 28.201 Ma Fish Canyon sanidine (Kuiper *et al.* 2008) using decay constants of Min *et al.* (2000).
$\pm 2\sigma_{an}$ denotes analytical uncertainty only at the 95% confidence interval. $\pm 2\sigma_{int}$ denotes analytical plus *J* uncertainty. $\pm 2\sigma_{ext}$ denotes fully propagated.
Uncertainty at the 95% confidence interval including analytical, *J*-value, standard age and decay constant contributions.
N = number of dates used in weighted mean/total number of single crystal fusion dates.
MSWD = mean square of weighted deviates.

of these bentonites in the *Didymoceras cheyennense* and *Baculites reesidei* Ammonite Zones, respectively. For example, whereas 92-O-31 yields a nearly unimodal population of dates, most exceed 75 Ma, which is older than the stratigraphically underlying *Exiteloceras jennyi* Zone dated at 74.67 ± 0.10/0.12/0.16 Ma (Table 1). Individual sanidine dates from 91-O-12 are too dispersed to calculate a weighted mean age (Fig. 4) and the youngest dates exceed the age of biostratigraphically younger strata. The reason these two bentonites contain largely older, inherited crystals is unclear, but these are not simple primary airfall beds and may represent redeposited ash, a challenge to dating such systems noted by Obradovich (1993). We report five new $^{40}Ar/^{39}Ar$ age determinations in Tables 1 and 2. We next summarize the radioisotopic ages that have been determined within each Cretaceous stage.

Albian stage

Within Albian strata, seven $^{40}Ar/^{39}Ar$ and three U–Pb age determinations range from 108.07 ± 0.05/0.10/0.20 Ma in the Hulcross Formation, British Columbia to 101.23 ± 0.05/0.09/0.18 Ma in the Muddy Sandstone, Wyoming (Table 1; Singer *et al.* 2021). Radioisotopic ages that most closely constrain the Aptian–Albian boundary from Europe include the $^{40}Ar/^{39}Ar$ age of 114.77 ± 0.15/0.17/0.26 Ma of bentonite in the uppermost Aptian *Paraholplites nutfieldensis* Ammonite Zone at Gott, Germany, and a U–Pb age of 113.08 ± 0.10/0.20/0.30 Ma from the Vohrum tuff, Germany, just above the *Leymeriella shrammeni anterior* Zone in lowermost Albian strata (Selby *et al.* 2009; Singer *et al.* 2021). The age of the Aptian–Albian boundary from spline fitting of marine magnetic anomalies in the *Geologic Time Scale 2020* is 113.2 ± 0.3 Ma (Gradstein *et al.* 2020).

Cenomanian stage

Seventeen $^{40}Ar/^{39}Ar$ and five U–Pb age determinations are from bentonitic ash beds in Cenomanian strata (Table 1). The three oldest $^{40}Ar/^{39}Ar$ ages within the Shell Creek Shale in Montana and Wyoming are 100.07 ± 0.03/0.07/0.17 Ma, 99.67 ± 0.11/0.13/0.20 Ma and 99.62 ± 0.03/0.07/0.17 Ma. The age of 99.67 ± 0.11/0.13/0.20 Ma is associated with fossils of *Neogastroplites haasi* near Greybull, Wyoming (Table 1), whereas the age of 100.07 ± 0.07 Ma is likely very close to the base of the Cenomanian (Singer *et al.* 2021). The *Geologic Time Scale 2020* gives an age of 100.5 ± 0.1 Ma for the base of the Cenomanian (Fig. 2; Gradstein *et al.* 2020). Other radioisotopic ages span from 99.58 ± 0.03/0.12/0.19 Ma in the Newcastle Sandstone, Wyoming through 93.99 ± 0.03/0.06/0.15 Ma and 93.98 ± 0.03/0.06/0.15 Ma for a correlative to bentonite B (Elder 1988) in the *Neocardioceros juddi* ammonite zone in the uppermost Cenomanian strata at the GSSP for the Cenomanian–Turonian boundary in Pueblo State Park, Colorado, and in Thayer County, Nebraska (Table 1). The age of the Albian–Cenomanian boundary cannot be ascertained from Western Interior Basin strata because diagnostic fossils are not present. However, the $^{40}Ar/^{39}Ar$ age of 100.0 ± 0.4 Ma determined by Obradovich *et al.* (2002) from a bentonite in the Yezo Group, Hokkaido, Japan, is associated with the first appearance of the planktonic formaniner species *Thalmanninella globotruncanoides* and we provisionally use this as the age of the Albian–Cenomanian boundary (Singer *et al.* 2021).

A different estimate for the age of the Albian–Cenomanian boundary (97.17 Ma) based on dinoflagellate biostratigraphy and sequence stratigraphy of the Texas Gulf Coast and Western Interior Basin was proposed by Scott *et al.* (2009). Although the

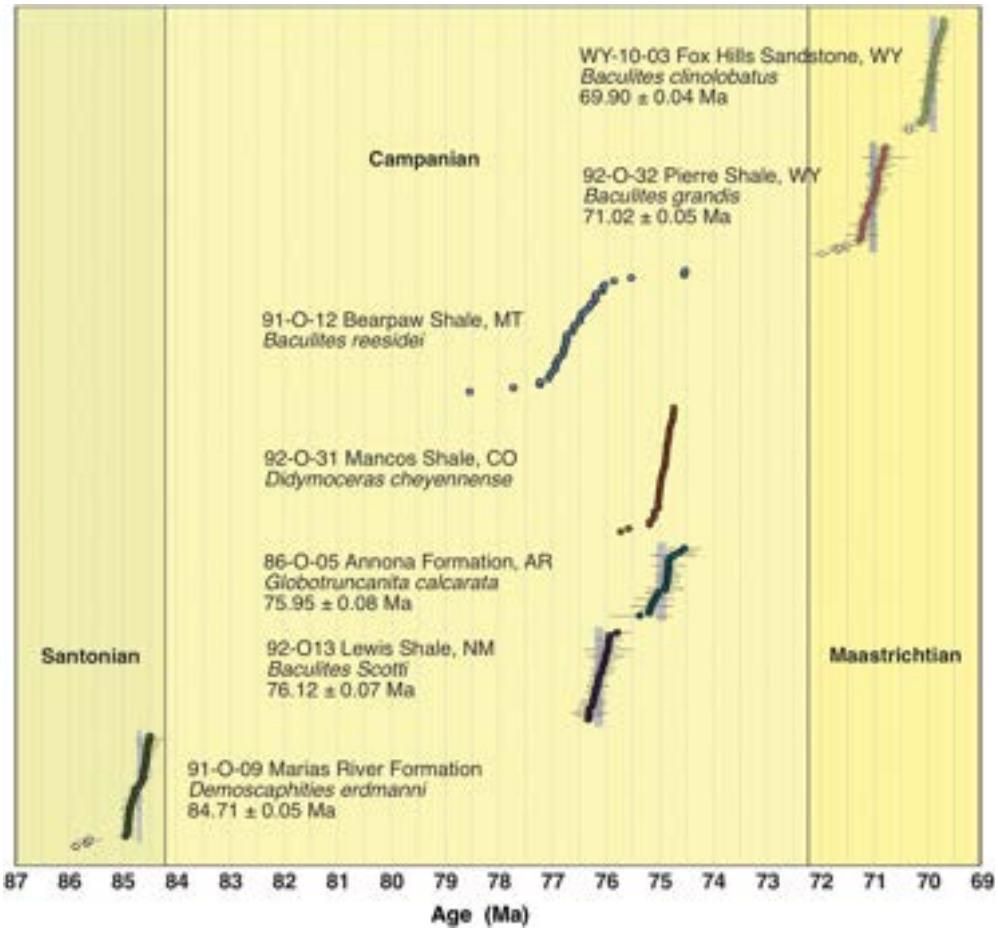

Fig. 4. Rank order plot of $^{40}Ar/^{39}Ar$ dates from sanidine in seven bentonite samples. Each individual date is shown with $\pm 1\sigma$ analytical uncertainty. The open symbols denote dates not used to calculate weighted mean ages, shown as vertical grey bars with $\pm 2\sigma$ analytical uncertainty as listed. Ages calculated relative to 28.201 Ma Fish Canyon sanidine (Kuiper *et al.* 2008) using the Min *et al.* (2000) decay constant.

authors recognized the >2 Myr disparity between their proposed age and the Obradovich *et al.* (2002) $^{40}Ar/^{39}Ar$ date of 100.0 ± 0.4 Ma from *T. globotruncanoides*-bearing strata of Japan, they implied that the offset might be attributable to issues with Obradovich's radioisotopic dating, such as differences between the time of crystallization and time of deposition of sanidine crystals, or to reworking of such crystals, rather than to any error in their age estimate. The authors clearly identified the discrepancy as a target for further study, but they did not rigorously evaluate potential sources of uncertainty in their biostratigraphic and sequence stratigraphic compilations (e.g. why the aforementioned dating issues would not also apply to any radioisotopic age determinations used to anchor biostratigraphic or sequence stratigraphic datums). A key factor not addressed by Scott *et al.* (2009) was the intercalibration of different radioisotopic age data, including recalibration of older $^{40}Ar/^{39}Ar$ dates using the currently accepted age for the Fish Canyon sanidine monitor. Singer *et al.* (2021) provide a comprehensive compilation of new precise age determinations and other published dates for the Aptian through Cenomanian, using standard statistical methods for geochronological analysis and address the issues raised above. The compiled data strongly support the Albian–Cenomanian boundary age proposed herein (100.0 ± 0.04 Ma).

Turonian stage

Twelve $^{40}Ar/^{39}Ar$ and three U–Pb age determinations range from 94.02 ± 0.14/0.15/0.20 Ma for a

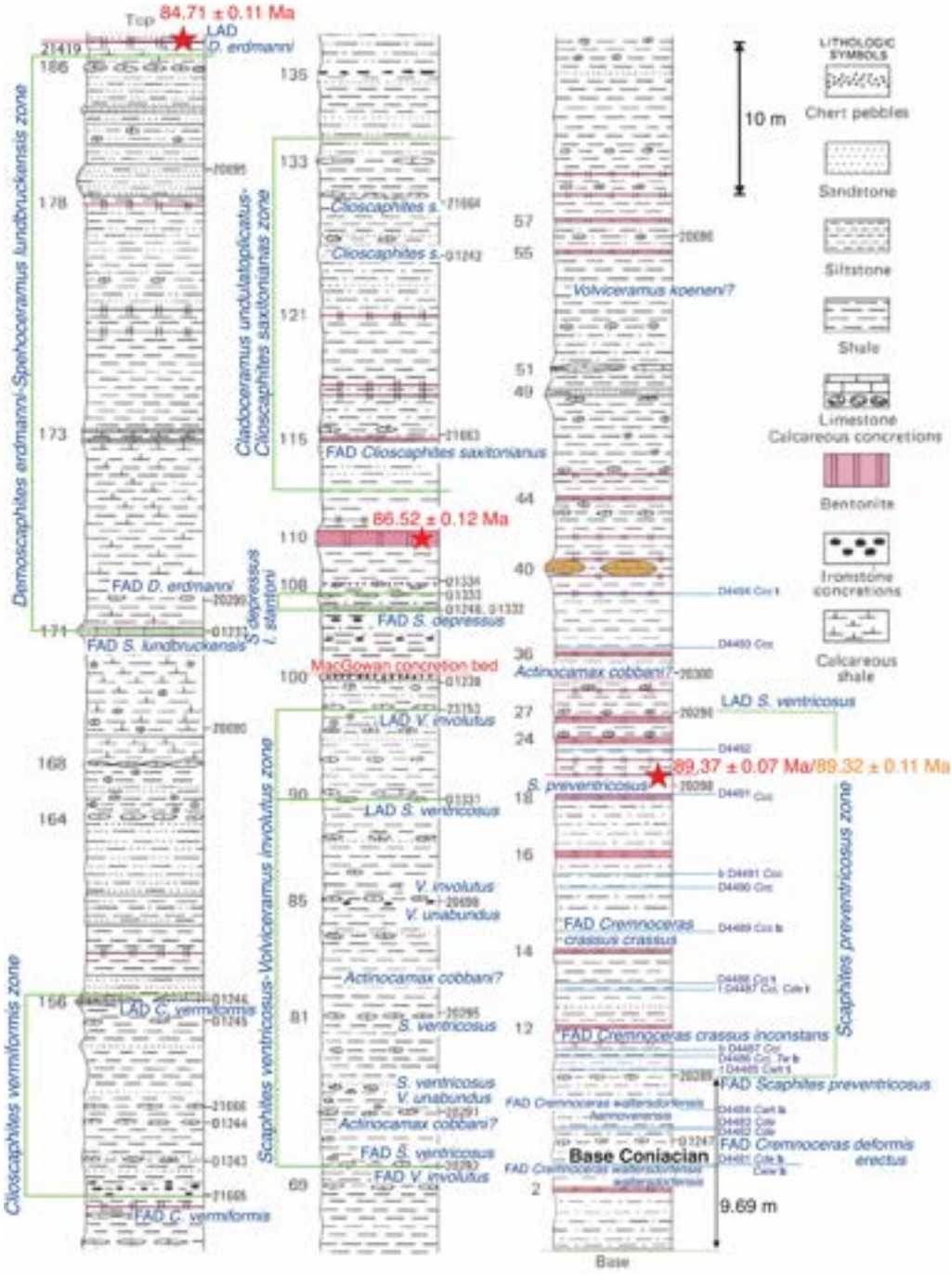

Fig. 5. Type section of the Kevin Member of the Marias River Shale near Kevin, Montana. Stars show position of three bentonites in this section with ages from Table 1. Source: modified after Cobban *et al.* (1976). Ammonite and inoceramid zones and USGS D numbers are from Cobban *et al.* (1976) and McKinney (2018).

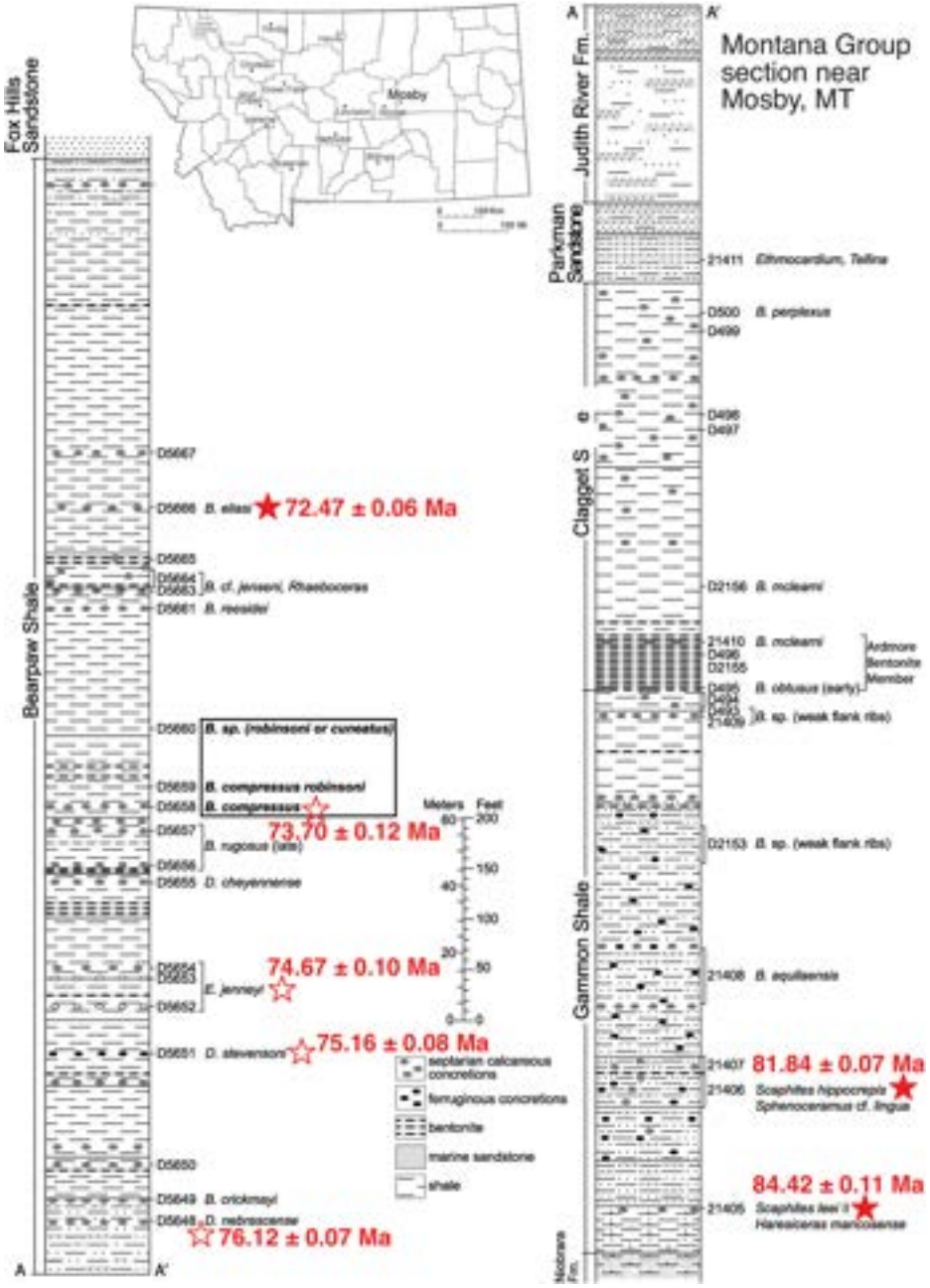

Fig. 6. Section near Mosby, Montana showing the entire thickness of the Montana Group, from the top of the Niobrara Formation (Colorado Group) to the Fox Hills Sandstone, including the Gammon Shale, Claggett Shale, Parkman Sandstone, nonmarine Judith River Formation and Bearpaw Shale. Filled stars are bentonites dated from localities relatively close to Mosby in Petroleum County, Montana. Open stars show ages correlated into this section. These include an age of 84.42 $\pm$ 0.12 Ma (weighted mean of the $^{40}Ar/^{39}Ar$ and U–Pb ages with the total uncertainties included) from McDonald Creek at Winnett (Denver Mesozoic D4912) that corresponds to the same stratigraphic level as the Washington Mesozoic locality 21405 at Mosby. The 81.84 $\pm$ 0.07 Ma age for the *Scaphites hippocrepis ii* Zone is from Cat Creek oil field area in Petroleum County, and represents a new location for the sample reported in Sageman *et al.* (2014). Source: modified from Landman *et al.* (2010, fig. 8).

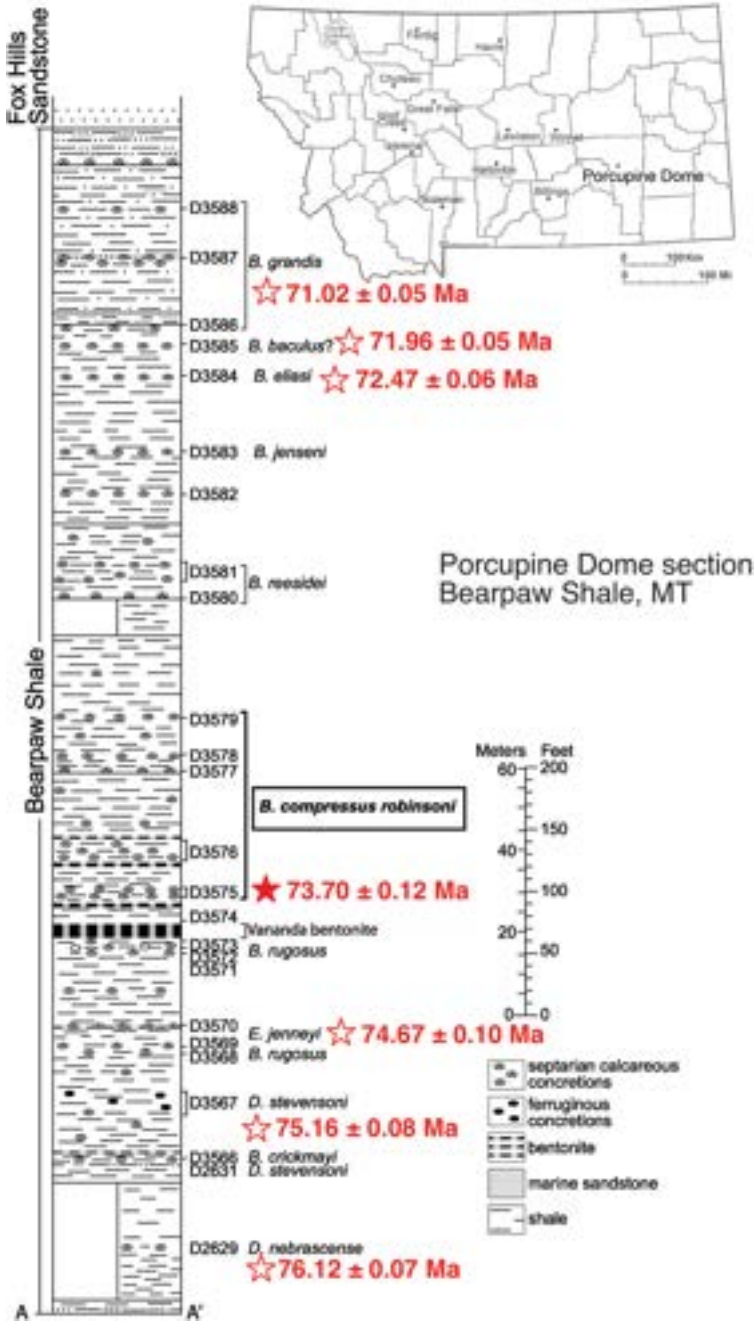

Fig. 7. Porcupine Dome section of the Bearpaw Shale of Landman *et al.* (2010). The bentonite sample 90-O-15 dated at 73.70 $\pm$ 0.12 Ma is from the base of the *Baculites compressus* Zone on the east bank of the Bighorn River in Bighorn County, Montana, about 100 km SW of Porcupine Dome. It was collected (Denver Mesozoic D number 13111) by W.A. Cobban and E.A. Merewether on 17 June 1990, and is 22 cm thick, the highest of three bentonites in the lower 5 m of the Bearpaw Shale. The other ages, shown as open stars, are from ammonite zones dated elsewhere in the Western Interior Basin, and are generally plotted in the middle of the correlative ammonite zone. Exceptions include bentonites in the *Baculites grandis* Zone (see discussion of Red Bird section, Wyoming) and at the boundary of the *Didymoceras nebracense* and *Baculites scotti* Zones from the San Juan Basin, New Mexico.

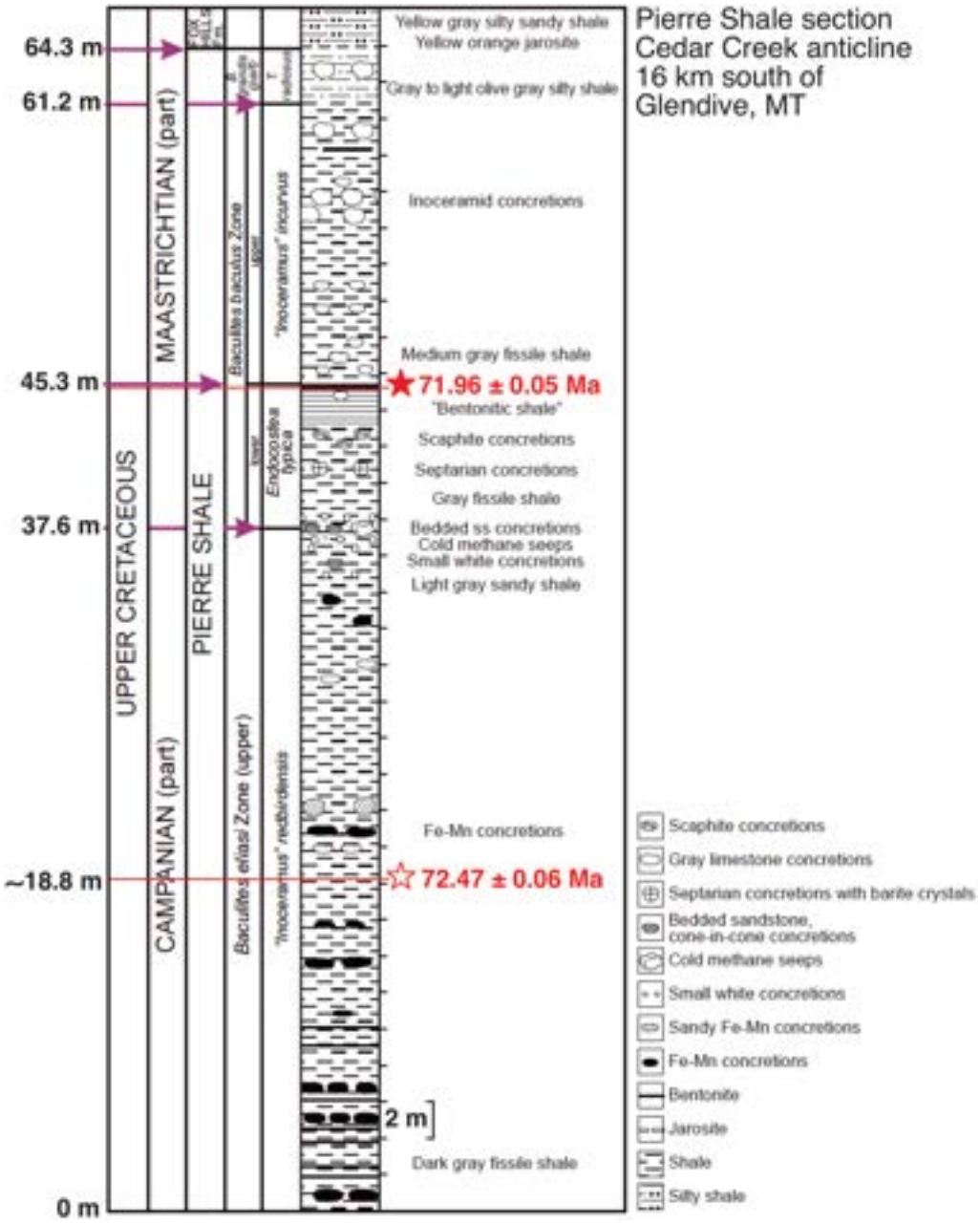

Fig. 8. Section of Pierre Shale on the Cedar Creek Anticline, 16 km south of Glendive, Montana, modified from Landman *et al.* (2020). Notably, the $^{40}Ar/^{39}Ar$ age of 71.96 $\pm$ 0.05 Ma of Landman *et al.* (2020) is from a bentonite that crops out one-third (32.7%) of the way up in the 23.26 m thick *Baculites baculus* Ammonite Zone in this section, and coincides with the first appearance of '*Inoceramus*' *incurvus*, the upper inoceramid subzone of the *B. baculus* Ammonite Zone. Potentially, this allows the first appearance of '*I.*' *incurvus* to be dated in correlative strata throughout the Western Interior Basin. The bentonite age of 72.47 $\pm$ 0.06 Ma shown as the open star, by contrast, is only approximately located in the centre of the *Baculites eliasi* Ammonite Zone in this section, as there is no specific information on the stratigraphic position of the bentonite in this ammonite zone where it was collected near Mosby, Montana (Fig. 6).

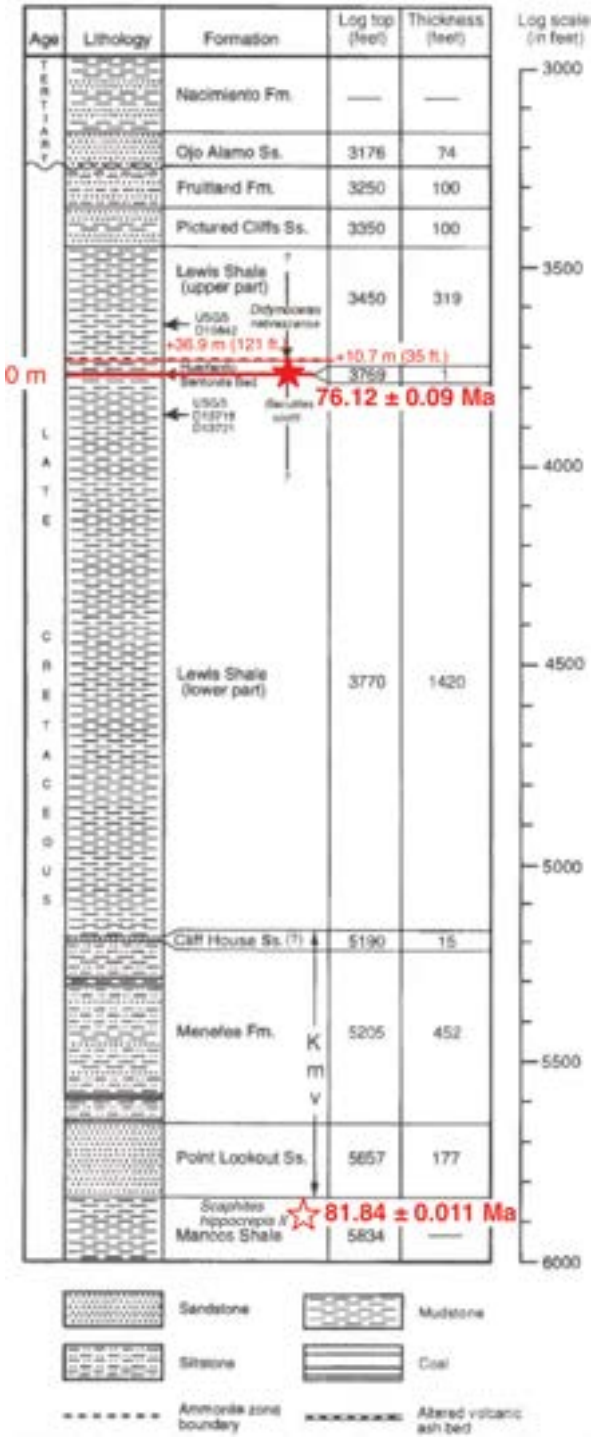

Fig. 9. Section comprising Campanian strata in Rio Arriba County, NM showing location of dated bentonites, including one in the upper portion of Lewis Shale at the boundary between the *Baculites scotti* and *Didymoceras nebrascense* Ammonite Zones. Source: modified from Fassett *et al.* (1997).

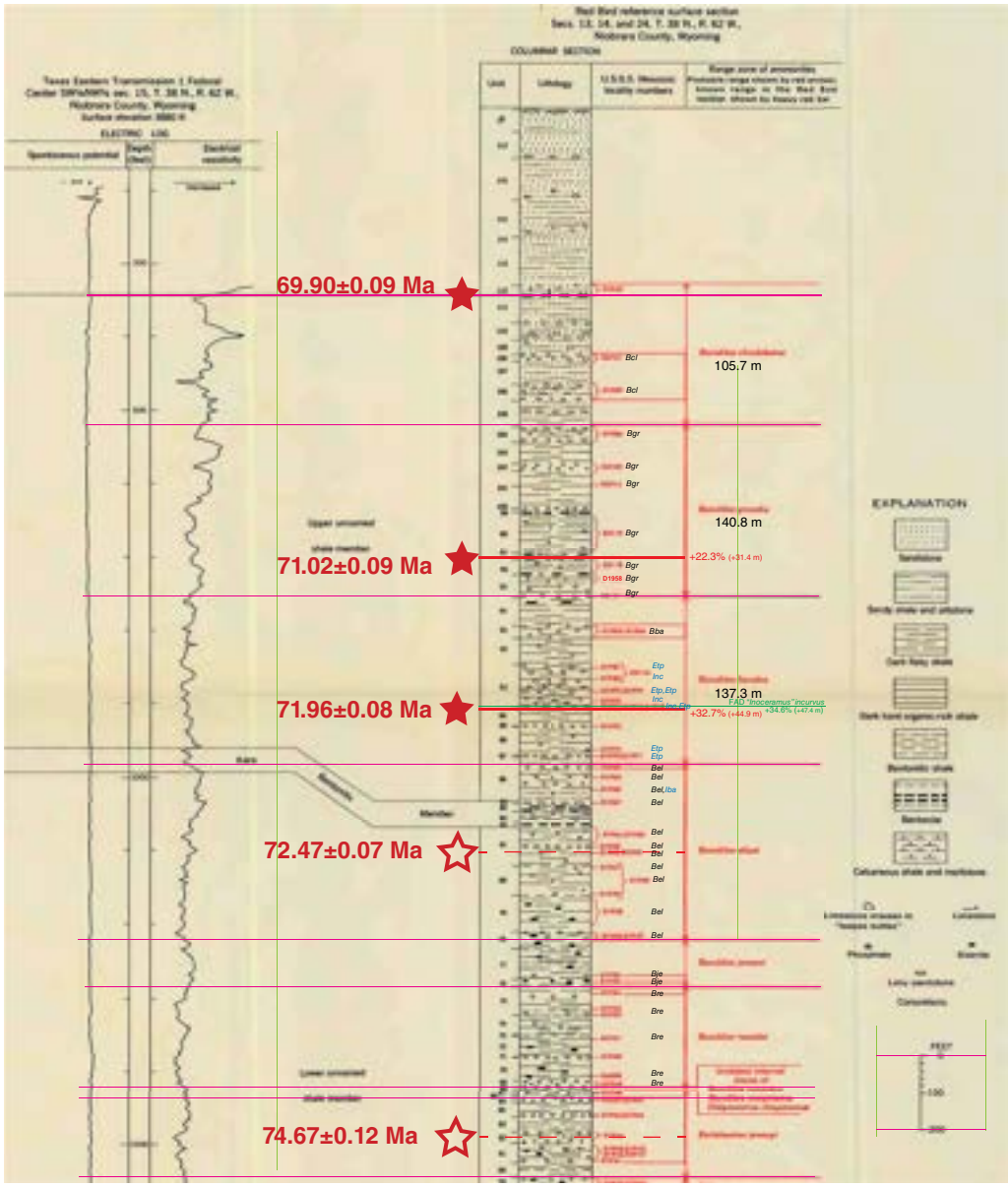

Fig. 10. Upper portion of the Red Bird, Wyoming, section modified to show the positions of three dated bentonites that can be projected into this section with confidence (filled red stars) and two (open stars) that are projected into the section at the mid-points of the *Baculities eliasi* and *Exiteloceras jenneyi* Zones from other localities. The latter two bentonites are from the Bearpaw Shale (Fig. 4) and the Pierre Shale in Pueblo County, Colorado (Table 1). Source: modified from Gill and Cobban (1966).

bentonite at the base of the Turonian global stratotype section in the *Watinoceras devonense* Ammonite Zone near Pueblo, Colorado, to 89.87 ± 0.06/0.10/0.16 Ma from a bentonite in the Marias River Shale, Montana that is associated with *Scaphites nigricollensis* ammonites (Table 1). The Cenomanian–Turonian boundary is placed at 93.95 ± 0.05 Ma on the basis of the age determinations summarized in Table 1 and Figure 3 (Jones *et al.* 2021) and improves upon precision of the 93.9 ± 0.2 Ma estimate in the *Geologic Time Scale 2020* (Gradstein *et al.* 2020; Fig. 2).

Coniacian stage

Three $^{40}Ar/^{39}Ar$ and two U–Pb age determinations span from 89.37 ± 0.07/0.15 Ma for a bentonite in the *Scaphites preventricosus* Ammonite Zone in Montana, to 86.52 ± 0.09/0.12/0.33 Ma from a bentonite in the Marias River Shale Formation near Kevin, Montana that is associated with *Scaphites depressus* ammonites (Table 1; Fig. 5). The Turonian–Coniacian boundary is placed at 89.75 ± 0.38 Ma on the basis of astronomical age models that leverage the age determinations summarized in Table 1 (Sageman *et al.* 2014) and is within uncertainty of the 89.4 ± 0.2 Ma estimate in the *Geologic Time Scale 2020* (Gradstein *et al.* 2020; Fig. 2).

Santonian stage

One U–Pb and four $^{40}Ar/^{39}Ar$ age determinations span from 85.84 ± 0.24/0.34 Ma for a bentonite in the *Cladoceramus undulatoplicatus* Inoceramid Zone in Texas to 84.41 ± 0.14/0.24 Ma from a bentonite in the Telegraph Creek Formation, Montana that is associated with *Demoscaphites bassleri* ammonites (Table 1). The Coniacian–Santonian boundary is placed at 86.49 ± 0.44 Ma on the basis of astronomical age models that leverage the age determinations summarized in Table 1 (Sageman *et al.* 2014) and is significantly older than the 85.7 ± 0.5 Ma estimate in the *Geologic Time Scale 2020* (Gradstein *et al.* 2020; Fig. 2).

Campanian stage

Two U–Pb and eight $^{40}Ar/^{39}Ar$ age determinations span from 81.84 ± 0.07/0.11/0.16 Ma for a bentonite in the *Scaphites hippocrepis ii* Ammonite Zone in Montana to 72.47 ± 0.06/0.07/0.12 Ma from a bentonite in the *Baculites eliasi* Ammonite Zone (Table 1). We locate several of these dated bentonites within the sections near Mosby, Porcupine Dome, and Glendive, Montana from Landman *et al.* (2010, 2018, 2020; Figs 6–8) and in the Lewis Shale, New Mexico (Fig. 9). The Santonian–Campanian boundary is placed at 84.19 ± 0.38 Ma on the basis of astronomical age models that leverage the age determinations summarized in Table 1 (Sageman *et al.* 2014) and is significantly older than the 83.7 ± 0.2 Ma estimate in the *Geologic Time Scale 2020* (Gradstein *et al.* 2020; Fig. 2).

Maastrichtian stage and end-Cretaceous

One U–Pb and three $^{40}Ar/^{39}Ar$ age determinations range from 71.96 ± 0.08 Ma for a bentonite in the *Baculites baculus* Ammonite Zone in Montana to 66.082 ± 0.02/0.04/0.08 Ma from a bentonite in uppermost Cretaceous sediment of the Denver Basin at the Bijou Creek section (Table 1). The Campanian–Maastrichtian boundary is loosely placed at 72.20 ± 0.20 Ma using the estimate from the *Geologic Time Scale 2020* (Gradstein *et al.* 2020; Fig. 2). The $^{40}Ar/^{39}Ar$ ages determined for three of these bentonites of 71.96 ± 0.05/0.08/0.13 Ma, 71.02 ± 0.05/0.09/0.13 Ma and 69.90 ± 0.04/0.09/0.13 Ma are placed in the *Baculites baculus*, *Baculites grandis* and just above the *Bacultites clinolobatus* zones, respectively, in the Red Bird, Wyoming, section of Gill and Cobban (1966; Fig. 10). A U–Pb age model based on dates from volcanic ash beds with a magneto-biostratigraphic framework in the Denver Basin gives an age of 66.02 ± 0.02/0.04/0.08 Ma for the Cretaceous–Paleogene boundary (Clyde *et al.* 2016). The latter age agrees well with the $^{40}Ar/^{39}Ar$ age of 65.821 ± 0.060/0.067 Ma from ash in the IrZ coal of the Hell Creek area in NE Montana (Table 1; Sprain *et al.* 2018) and the age for the Cretaceous–Paleogene boundary of 65.85 ± 0.02/0.11 Ma inferred by Sprain *et al.* (2018).

Discussion

The broad distribution of many ammonite species, plus the pandemic biogeographic character of the majority of inoceramid taxa of the Albian–Upper Cretaceous succession of the North American Western Interior Basin provide high potential for the direct biostratigraphic transfer of the radioisotopic ages assembled herein to other localities around the globe.

At the stage level, the base of the Turonian is radioisotopically dated in the Pueblo GSSP section, and the age is within the range of *Mytiloides puebloensis* Walaszczyk and Cobban, an early member of the *Mytiloides labiatus* lineage, known worldwide. Inoceramids allow for the direct transfer of the Western Interior radioisotopic ages for both the bases of the Coniacian and Santonian stages, with each boundary defined by the evolutionary appearance of the index inoceramids (see Lamolda *et al.* 2014 and Walaszczyk *et al.* 2022, respectively). The age 89.37 ± 0.07/0.15 Ma for a bentonite in the *Scaphites preventricosus* Ammonite Zone in Montana is indistinguishable from the 89.4 ± 0.2 Ma estimate in the *Geologic Time Scale 2020* (Gradstein *et al.* 2020). Similarly, the age 85.84 ± 0.23/0.24/0.27 Ma for a bentonite in the *Cladoceramus undulatoplicatus* Inoceramid Zone in Texas approximates closely the 85.7 ± 0.2 Ma estimate in the *Geologic Time Scale 2020* (Gradstein *et al.* 2020). Moreover, inoceramids allow for the approximate age transfer for the base of the Maastrichtian, associated with the evolutionary appearance of *Endocostea typica*, a species well represented in

the entire Euramerican biogeographical region (Walaszczyk *et al.* 2001). Current attempts at redefinition of this boundary (a new Maastrichtian working group aimed at this task was established during the 2022 Cretaceous Symposium in Warsaw, Poland) may find the inoceramid-based definition the most suitable one.

Inoceramids may become helpful in the transfer of radioisotopic ages also at the substage level. Although there is no formal substage level subdivision of the Upper Cretaceous, numerous levels are traditionally treated as such.

The 95.39 ± 0.16/0.18/0.23 Ma radioisotopic age for the bentonite in the *Dunveganoceras pondi* Ammonite Zone dates the *Inoceramus prefragilis* Inoceramid Zone, which marks the appearance level of the *Inoceramus pictus* lineage. The appearance of this lineage is well recorded worldwide and potentially may be selected as the base of the upper Cenomanian. The lineage is well represented in the North American Western Interior, Europe, India, Madagascar and in the North Pacific Province (Gale *et al.* 2002).

The radioisotopic ages of 87.11 ± 0.08/0.15 Ma and 87.13 ± 0.07/0.09/0.18 Ma for bentonites in the *Scaphites depressus* Ammonite Zone in Montana, correspond with the *Sphenoceramus subcardissoides* Inoceramid Zone (see Landman *et al.* 2017; Walaszczyk *et al.* 2017), the marker for the upper Coniacian, within the Euramerican Biogeographic Province.

Among the Coniacian ages, of particular importance is the radioisotopic age 86.52 ± 0.09/0.12/0.17 Ma from bentonite bed 110 in the Kevin Member of the Marias River Shale Formation near Kevin, Montana (Fig. 5). Based on geophysical correlations (Plint *et al.* 2017), this bentonite is located very close to the Coniacian–Santonian boundary (with most of the upper Coniacian missing), as defined with the first appearance of the ammonite *Scaphites saxitonianus*, the widely used marker of the base of the Santonian in the North American Western Interior. The first appearance of this taxon, as dated against *Cladoceramus undulatoplicatus*, the formal marker of the base of the Santonian, approximates well the base of the Santonian (e.g. Walaszczyk and Cobban 2006, 2007). This age is almost identical to the 86.49 ± 0.44 Ma base Santonian age, based on the astronomical age models of Sageman *et al.* (2014).

Several published and newly reported radioisotopic ages are associated with inoceramid occurrences within the upper Campanian and lower Maastrichtian (Table 1). Of importance in stratigraphic correlation is the $^{40}Ar/^{39}Ar$ age of 75.16 ± 0.08/0.12/0.16 Ma for the bentonite in the *Didymoceras stevensoni* Ammonite Zone, which marks the lower part of the *Sphaeroceramus pertenuiformis* Inoceramid Zone. The latter is well recognized within the Euramerican Biogeographic Province, and may potentially be selected as the base of the upper Campanian substage, in the tripartite subdivsion scheme of this stage. Moreover, radioisotopic ages in Table 1 are associated with the inoceramid zones of '*Inoceramus*' *altus*, '*Inoceramus*' *redbirdensis* and *Trochoceramus radiosus*, each recognized widely within the Euramerican Biogeographic Province; the latter taxon is known also outside the province, in India and South Africa (Walaszczyk *et al.* 2009).

Conclusions and future directions

Building on the exceptionally collaborative and ground-breaking work of William A. Cobban and John D. Obradovich, 57 $^{40}Ar/^{39}Ar$ sanidine and 17 U–Pb zircon ages have been determined during the last decade for bentonitic ash beds in the marine strata of the Western Interior Basin that range from the early Albian at 108 Ma to the end-Cretaceous at 66 Ma. Six bentonites that occur within the *Vascoceras diartianum, Neocardiocerus juddi, Prionocylus macombi, Scaphites preventricosus, Scaphites depressus* and *Desmoscaphites bassleri* Ammonite Zones are dated using both methods and yield $^{40}Ar/^{39}Ar$ and U–Pb ages in agreement to within 150 kyr (or much less), which is comparable to currently achievable analytical uncertainties. Ages of these six bentonites form the backbone of the Western Interior Basin timescale and reinforce the close intercalibration of the $^{40}Ar/^{39}Ar$ and U–Pb chronometers.

We anticipate further refinements in the integration of biostratigraphy and radioisotopic dating of the Upper Cretaceous Western Interior Basin in the coming years. Because of ongoing taxonomic revisions in ammonites, inoceramids and foraminifera, coupled with additional field work, the biostratigraphic framework is becoming better established. One of the important challenges in radioisotopic dating is reviewing and pinpointing the locations of the bentonites used in previous studies, with respect to their position within each zone. We are also searching for additional bentonites from other parts of the section that have not been adequately sampled, such as the upper Maastrichtian. At the same time, advances in analytical techniques and the use of widely accepted standards are leading to improvements in the reproducibility of the age determinations. All these efforts contribute to the progressive refinement of the chronostratigraphic framework of the Upper Cretaceous Western Interior Basin and enhance its utility for global correlation.

Acknowledgements This contribution would not have been possible without the generous support and advice of John Obradovich and William Cobban of the US

Geological Survey and we are grateful for their inspiration. We thank Bryan Wathen and Youjuan Li for laboratory assistance. The thorough and insightful review by Robert Hildebrand is greatly appreciated.

Competing interests The authors declare that they have no known competing financial interests or personal relationships that could have appeared to influence the work reported in this paper.

Author contributions **BSS**: conceptualization (lead), funding acquisition (lead), investigation (lead), methodology (lead), project administration (lead), supervision (lead), visualization (equal), writing – original draft (lead), writing – review & editing (equal); **BRJ**: data curation (lead), formal analysis (equal), methodology (supporting), writing – review & editing (supporting); **DAS**: conceptualization (supporting), investigation (equal), visualization (equal), writing – review & editing (supporting); **IW**: investigation (supporting), methodology (supporting), visualization (supporting), writing – original draft (equal), writing – review & editing (supporting); **NL**: investigation (equal), visualization (supporting), writing – original draft (supporting), writing – review & editing (supporting); **BBS**: conceptualization (supporting), investigation (supporting), writing – review & editing (supporting); **KCM**: data curation (supporting), investigation (supporting).

Funding Supported in part by United States National Science Foundation grants # EAR-1951812 and EAR-1951835 and by Polish National Science Centre grant # 2018/31/B/ST10/01820.

Data availability All data are available in the Supplementary Material or in the original publications cited.

References

Barker, I.R., Moser, D.E., Kamo, S.L. and Plint, A.G. 2011. High-precision U–Pb zircon ID–TIMS dating of two regionally extensive bentonites: Cenomanian Stage, Western Canada Foreland Basin. *Canadian Journal of Earth Sciences*, **48**, 543–556, https://doi.org/10.1139/E10-042

Batenburg, S.J., De Vleeschouwer, D. *et al*. 2016. Orbital control on the timing of oceanic anoxia in the Late Cretaceous. *Climate of the Past Discussions*, **12**, 1995–2009, https://doi.org/10.5194/cp-12-1995-2016

Clyde, W.C., Ramezani, J., Johnson, K.R., Bowring, S.A. and Jones, M.M. 2016. Direct high-precision U–Pb geochronology of the end-Cretaceous extinction and calibration of Paleocene astronomical timescales. *Earth and Planetary Science Letters*, **452**, 272–280, https://doi.org/10.1016/j.epsl.2016.07.041

Cobban, W.A. 1958*a*. Two new species of *Baculites* from the Western Interior region. *Journal of Paleontology*, **32**, 660–665.

Cobban, W.A. 1958*b*. Late Cretaceous fossil zones of the Powder River basin, Wyoming and Montana. *AAPG 13th Annual Field Conference Guidebook*, 114–119.

Cobban, W.A. and Hook, S.C. 1979. *Collignoniceras woollgari woollgari* (Mantell) ammonite fauna from Upper Cretaceous of Western Interior, United States. *Memoir of the New Mexico Bureau of Mines & Mineral Resources*, **37**.

Cobban, W.A. and Reeside, J.B., Jr. 1952. Correlation of the Cretaceous formations of the Western Interior of the United States. *Geological Society of America Bulletin*, **63**, 1011–1044, https://doi.org/10.1130/0016-7606(1952)63[1011:COTCFO]2.0.CO;2

Cobban, W.A., Erdmann, C.E., Lemke, R.W. and Maughan, E.K. 1976. Type sections and stratigraphy of the members of the Blackleaf and Marias River Formations (Cretaceous) of the Sweetgrass Arch, Montana. *United States Geological Survey Professional Paper* **974**. US Government Printing Office.

Cobban, W.A., Walaszczyk, I., Obradovich, J.D. and McKinney, K.C. 2006. A USGS zonal table for the Upper Cretaceous Middle Cenomanian-Maastrichtian of the Western Interior of the United States based on ammonites, inoceramids, and radiometric Ages. *U.S. Geological Survey, Open-File Report 2006-1250*, https://doi.org/10.3133/ofr20061250

Condon, D., Bowring, J.F. *et al*. 2016. The Earthtime initiative: accelerating advances in geochronology since 2003. *Geological Society of America Abstracts with Programs, 48*, Denver, CO, https://doi.org/10.1130/abs/2016AM-282709

Elder, W.P. 1988. Geometry of Upper Cretaceous bentonite beds: implications about volcanic source areas and paleowind patterns, Western Interior, United States. *Geology*, **16**, 835–838, https://doi.org/10.1130/0091-7613(1988)016<0835:GOUCBB>2.3.CO;2

Eldrett, J.S., Ma, C. *et al*. 2015. An astronomically calibrated stratigraphy of the Cenomanian, Turonian and earliest Coniacian from the Cretaceous Western Interior Seaway, USA: Implications for global chronostratigraphy. *Cretaceous Research*, **56**, 316–344, https://doi.org/10.1016/j.cretres.2015.04.010

Fassett, J.E., Cobban, W.A. and Obradovich, J.D. 1997. Biostratigraphic and isotopic age of the Huerfanito bentonite bed of the Upper Cretaceous Lewis Shale at an outcrop near Regina, New Mexico. *In*: Anderson, O., Kues, B.S. and Lucas, S.G. (eds) *Mesozoic Geology and Paleontology of the Four Corners Region*. New Mexico Geological Society, 48th Annual Field Conference Guidebook. New Mexico Geological Society, 229–232.

Gale, A.S., Hardenbol, J., Hathway, B., Kennedy, W.J., Young, J.R. and Phansalkar, V. 2002. Global correlation of Cenomanian (Upper Cretaceous) sequences: evidence for Milankovitch control on sea level. *Geology*, **30**, 291–294, https://doi.org/10.1130/0091-7613(2002)030<0291:GCOCUC>2.0.CO;2

Gill, J.R. and Cobban, W.A. 1966. The Red Bird section of the Upper Cretaceous Pierre Shale in Wyoming. *USGS Professional Paper* **393**. US Government Printing Office.

Gradstein, F.M., Ogg, J.G., Schmitz, M. and Ogg, G. (eds) 2012. *The Geologic Time Scale 2012*. Elsevier.

Gradstein, F.M., Ogg, J.G., Schmitz, M.D. and Ogg, G.M. (eds) 2020. *Geologic Time Scale 2020*. Elsevier.

Hancock, J.M. 1984. Some possible boundary-stratotypes for the base of the Cenomanian and Turonian Stages. *Bulletin of the Geological Society of Denmark*, **33**, 123–128, https://doi.org/10.37570/bgsd-1984-33-10

Hattin, D.E. 1975. Stratigraphy and depositional environment of Greenhorn Limestone (Upper Cretaceous) of Kansas. *Kansas Geological Survey Bulletin*, **209**, 1–128.

Hicks, J.F., Obradovich, J.D. and Tauxe, L. 1999. Magnetostratigraphy, isotopic age calibration and intercontinental correlation of the Red Bird section of the Pierre Shale, Niobrara County, Wyoming, USA. *Cretaceous Research*, **20**, 1–27, https://doi.org/10.1006/cres.1998.0133

Hicks, J.F., Johnson, K.R., Obradovich, J.D., Tauxe, L., Clark, D., Hartman, J.H. and Nichols, D.J. 2002. Magnetostratigraphy and geochronology of the Hell Creek and basal Fort Union Formations of southwestern North Dakota and a recalibration of the age of the Cretaceous–Tertiary boundary. *Geological Society of America Special Paper*, **361**, 35–55, https://doi.org/10.1130/0-8137-2361-2.35

Jicha, B.R., Singer, B.S. and Sobol, P. 2016. Re-evaluation of the ages of $^{40}Ar/^{39}Ar$ sanidine standards and supereruptions in the western US using a Noblesse multicollector mass spectrometer. *Chemical Geology*, **431**, 54–66, https://doi.org/10.1016/j.chemgeo.2016.03.024

Jones, M.M., Sageman, B.B., Selby, D., Jicha, B.R., Singer, B.S. and Titus, A.L. 2021. Regional chronostratigraphic synthesis of the Cenomanian–Turonian Oceanic Anoxic Event 2 (OAE2) interval, Western Interior Basin (USA): New Re–Os chemostratigraphy and $^{40}Ar/^{39}Ar$ geochronology. *Geological Society of America Bulletin*, **133**, 1090–1104, https://doi.org/10.1130/B35594.1

Joo, Y.J. and Sageman, B.B. 2014. Cenomanian to Campanian carbon isotope chemostratigraphy from the Western Interior Basin, U.S.A. *Journal of Sedimentary Research*, **84**, 529–542, https://doi.org/10.2110/jsr.2014.38

Kauffman, E.G. 1975. Dispersal and biostratigraphic potential of Cretaceous benthonic bivalvia in the Western Interior. *Geological Association of Canada, Special Paper*, **13**, 163–194.

Kauffman, E.G., Cobban, W.A. and Eicher, D.L. 1978. Albian through Lower Coniacian strata, biostratigraphy and principal events, Western Interior United States. *Annales du Museum d'Histoire Naturelle de Nice*, **IV**, XXIII1–XXIII52.

Kauffman, E.G., Sageman, B.B., Kirkland, J.I., Elder, W.P., Harries, P.J. and Villamil, T. 1993. Molluscan biostratigraphy of the Cretaceous western interior basin, North America. *Geological Association of Canada Special Paper*, **39**, 397–434.

Kennedy, W.J. and Cobban, W.A. 1991. Stratigraphy and interregional correlation of the Cenomanian-Turonian transition in the Western Interior of the United States near Pueblo, Colorado, a potential boundary stratotype for the base of the Turonian stage. *Newsletters on Stratigraphy*, **24**, 1–33, https://doi.org/10.1127/nos/24/1991/1

Kennedy, W.J., Cobban, W.A. and Landman, N.H. 2001. A revision of the Turonian members of the ammonite subfamily Collignoniceratinae from the United States Western Interior and Gulf Coast. *Bulletin of the American Museum of Natural History*, **267**, 1–148, https://doi.org/10.1206/0003-0090(2001)267<0001:AROTTM>2.0.CO;2

Kirkland, J.I. 1991. Lithostratigraphic and biostratigraphic framework for the Mancos Shale (late Cenomanian to middle T uronian) at Black Mesa, northeastern Arizona in. Nations, J. D. and Eaton, J. F. (eds) *Stratigraphy, depositional environments, and sedimentary tectonics of the western margin, Cretaceous Western Interior Seaway*, **260**, 85–111.

Kuiper, K.F., Deino, A., Hilgen, F.J., Krijgsman, W., Renne, P.R. and Wijbrans, J.R. 2008. Synchronizing rock clocks of Earth history. *Science (New York, NY)*, **320**, 500–504, https://doi.org/10.1126/science.1154339

Kynaston, D., Bhattacharya, J.P., Singer, B.S. and Jicha, B.R. 2021. Facies architecture and time stratigraphic relationships of a confined trunk-tributary valley fill and unconfined fluvial system in the backwater of the Turonian Ferron-Notom Delta, Utah, USA. *Journal of Sedimentary Research*, **91**, 66–91, https://doi.org/10.2110/jsr.2020.76

Lamolda, M.A., Paul, C.R.C., Peryt, D. and Pons, J.M. 2014. The global boundary stratotype and section point (GSSP) for the base of the Santonian Stage, 'Cantera de Margas', Olazagutia, northern Spain. *Episodes*, **37**, 2–13, https://doi.org/10.18814/epiiugs/2014/v37i1/001

Landman, N.H. and Waage, K.M. 1993. Morphology and environment of Upper Cretaceous (Maastrichtian) *Scaphites*. *Geobios*, **26**, 257–265, https://doi.org/10.1016/S0016-6995(06)80380-3

Landman, N.H., Kennedy, W.J., Cobban, W.A. and Larson, N.L. 2010. Scaphites of the 'nodosus group' from the Upper Cretaceous (Campanian) of the Western Interior of North America. *Bulletin of the American Museum of Natural History*, **2010**, 1–242.

Landman, N.H., Plint, A.G. and Walaszczyk, I. 2017. Scaphitid ammonites from the Upper Cretaceous (Coniacian-Santonian) western Canada foreland basin. *Bulletin of the American Museum of Natural History*, **414**, 105–172, https://doi.org/10.1206/0003-0090-414.1.1

Landman, N.H., Jicha, B.R., Cochran, J.K., Garb, M.P., Brophy, S.K., Larson, N.L. and Brezina, J. 2018. $^{40}Ar/^{39}Ar$ date of a bentonite associated with a methane seep deposit in the upper Campanian *Baculites compressus* Zone, Pierre Shale, South Dakota. *Cretaceous Research*, **90**, 90–96, https://doi.org/10.1016/j.cretres.2018.03.024

Landman, N.H., Kennedy, W.J. *et al.* 2020. Large scaphitid ammonites (*Hoploscaphites*) from the Upper Cretaceous (Upper Campanian–Lower Maastrichtian) of North America: endless variation on a single theme. *Bulletin of the American Museum of Natural History*, **441**, 1–131, https://doi.org/10.1206/0003-0090.441.1.1

Lee, J.-Y., Marti, K., Severinghaus, J.P., Kawamura, K., Yoo, H.-S., Lee, J.B. and Kim, J.S. 2006. A redetermination of the isotopic abundance of atmospheric Ar. *Geochimica et Cosmochimica Acta*, **70**, 4507–4512, https://doi.org/10.1016/j.gca.2006.06.1563

Li, Y., Qin, H. *et al.* 2023. Revised onset age of magnetochron M0r: chronostratigraphic and geologic

implications. *Geology*, **51**, 565–570, https://doi.org/10.1130/G50873.1

Lin, W., Bhattacharya, J.P., Jicha, B.R., Singer, B.S. and Matthews, W. 2021. Has Earth ever been ice-free? Implications for glacio-eustasy in the Cretaceous greenhouse age using high-resolution sequence stratigraphy. *Geological Society of America Bulletin*, **133**, 243–252, https://doi.org/10.1130/B35582.1

Ma, C., Meyers, S.R., Sageman, B.B., Singer, B.S. and Jicha, B.R. 2014. Testing the astronomical time scale for oceanic anoxic event 2, and its extension into Cenomanian strata of the Western Interior Basin (USA). *Geological Society of America Bulletin*, **126**, 974–989, https://doi.org/10.1130/B30922.1

McKinney, K.C. 2018. *USGS Denver Mesozoic Catalog for 14595 fossil localities from the Rocky Mountain Region (1933–2017) [Data set]*. US Geological Survey, https://doi.org/10.5066/F7057F62

Mercer, C.M. and Hodges, K.V. 2016. ArAR–a software tool to promote the robust comparison of K–Ar and $^{40}Ar/^{39}Ar$ dates published using different decay, isotopic, and monitor-age parameters. *Chemical Geology*, **440**, 148–163, https://doi.org/10.1016/j.chemgeo.2016.06.020

Meyers, S.R., Siewert, S.E. *et al*. 2012. Intercalibration of radioisotopic and astrochronologic time scales for the Cenomanian/Turonian boundary Interval, Western Interior Basin, USA. *Geology*, **40**, 7–10, https://doi.org/10.1130/G32261.1

Miall, A.D., Catuneanu, O., Vakarelov, B.K. and Post, R. 2008. The Western interior basin. *Sedimentary Basins of the World*, **5**, 329–362, https://doi.org/10.1016/S1874-5997(08)00009-9

Min, K., Mundil, R., Renne, P.R. and Ludwig, K.R. 2000. A test for systematic errors in $^{40}Ar/^{39}Ar$ geochronology through comparison with U/Pb analysis of a 1.1-Ga rhyolite. *Geochimica et Cosmochimica Acta*, **64**, 73– 98, https://doi.org/10.1016/S0016-7037(99)00204-5

Oboh-Ikuenobe, F., Holbrook, J.M., Scott, R.W., Akins, S.L., Evetts, M.J., Benson, D.G. and Pratt, L.M. 2008. Anatomy of epicontinental flooding: Late Albian–Early Cenomanian of the southern US Western Interior Basin. *Geological Association of Canada, Special Paper*, **48**, 201–227.

Obradovich, J.D. 1993. A Cretaceous time scale. *Geological Association of Canada, Special Paper*, **39**, 379–396.

Obradovich, J.D. and Cobban, W.A. 1975. A time-scale for the Late Cretaceous of the Western Interior of North America. *Geological Association of Canada, Special Paper*, **13**, 31–45.

Obradovich, J.D., Matsumoto, T., Nishida, T. and Inoue, Y. 2002, Integrated biostratigraphic and radiometric study on the Lower Cenomanian (Cretaceous) of Hokkaido, Japan. *Proceedings of the Japan Academy Series B, Physical and Biological Sciences*, **78**, 149–153, https://doi.org/10.2183/pjab.78.149

Plint, A.G., Hooper, E.A. *et al*. 2017. Integrated, high-resolution allostratigraphic, biostratigraphic and carbon-isotope correlation of Coniacian strata (Upper Cretaceous), Western Alberta and northern Montana. *Bulletin of the American Museum of Natural History*, **414**, 9–52, https://doi.org/10.1206/0003-0090-414.1.3

Ramezani, J., Beveridge, T.L., Rogers, R.R., Eberth, D.A. and Roberts, E.M. 2022. Calibrating the zenith of dinosaur diversity in the Campanian of the Western Interior Basin by CA-ID-TIMS U–Pb geochronology. *Scientific Reports*, **12**, 16026, https://doi.org/10.1038/s41598-022-19896-w

Renaut, R.K., Tucker, R.T., Ryan King, M., Crowley, J.L., Hyland, E.G. and Zanno, L.E. 2023. Dating the Greenhorn transgression and OAE2 of the Western Interior Seaway in central Utah: implications for the absolute age of the Cenomanian-Turonian boundary. *Cretaceous Research*, **146**, 105464, https://doi.org/10.1016/j.cretres.2022.105464

Renne, P.R., Deino, A.L. *et al*. 2013. Time scales of critical events around the Cretaceous-Paleogene boundary. *Science (New York, NY)*, **339**, 684–687, https://doi.org/10.1126/science.1230492

Robinson, C.S., Mapel, W.J. and Cobban, W.A. 1959. Pierre Shale along western and northern flanks of Black Hills, Wyoming and Montana. *AAPG Bulletin*, **43**, 101–123.

Sageman, B.B., Singer, B.S. *et al*. 2014. Integrating $^{40}Ar/^{39}Ar$, U–Pb, and astronomical clocks in the Cretaceous Niobrara Formation, Western Interior Basin, USA. *Geological Society of America Bulletin*, **126**, 956–973, https://doi.org/10.1130/B30929.1

Schaen, A.J., Jicha, B.R. *et al*. 2021. Interpreting and reporting $^{40}Ar/^{39}Ar$ geochronologic data. *Geological Society of America Bulletin*, **133**, 461–487, https://doi.org/10.1130/B35560.1

Schaltegger, U., Ovtcharova, M. *et al*. 2021. Long-term repeatability and interlaboratory reproducibility of high-precision ID-TIMS U–Pb geochronology. *Journal of Analytical Atomic Spectrometry*, **36**, 1466–1477, https://doi.org/10.1039/D1JA00116G

Schmitz, M.D. 2012. Radiogenic isotope geochronology. *In*: Gradstein, F.M., Ogg, J.G., Schmitz, M. and Ogg, G. (eds) *The Geologic Time Scale*. Elsevier, 115–126.

Schmitz, M.D. and Kuiper, K.F. 2013. High-precision geochronology. *Elements*, **9**, 25–30, https://doi.org/10.2113/gselements.9.1.25

Schmitz, M.D., Singer, B.S. and Rooney, A.D. 2020. Radioisotope geochronology. *In*: Gradstein, F.M., Ogg, J.G., Schmitz, M.D. and Ogg, G.M. (eds) *Geologic Time Scale 2020*. Elsevier, 193–209.

Scott, G.R. and Cobban, W.A. 1965. *Geologic and Biostratigraphic Map of the Pierre Shale between Jarre Creek and Loveland*. US Geological Survey Miscellaneous Geologic Investigations Map I-439, scale, 1(480000), Colorado.

Scott, G.R. and Cobban, W.A. 1975. *Geologic and Biostratigraphic Map of the Pierre Shale in the Canon City-Florence Basin and the Twelvemile Park Area, south-central Colorado (No. 937)*. US Geological Survey.

Scott, G.R. and Cobban, W.A. 1986*a*. *Geologic and Biostratigraphic Map of the Pierre Shale in the Colorado Springs-Pueblo area, Colorado (No. 1627)*. US Geological Survey.

Scott, G.R. and Cobban, W.A. 1986*b*. *Geologic, Biostratigraphic, and Structure Map of the Pierre Shale between Loveland and Round Butte, Colorado (No. 1700)*. US Geological Survey.

Scott, R.W., Oboh-Ikuenobe, F.E., Benson, D.G., Jr and Holbrook, J.M. 2009. Numerical age calibration of the Albian/Cenomanian boundary. *Stratigraphy*, **6**, 17–32.

Seitz, O. 1956. Über Ontogenie, Variabilität und Biostratigraphie einiger Inoceramen. *Paläontologische Zeitschrift*, **30**, 3–6, https://doi.org/10.1007/BF0 3041763

Selby, D., Mutterlose, J. and Condon, D.J. 2009. U–Pb and Re–Os geochronology of the Aptian/Albian and Cenomanian/Turonian stage boundaries: implications for timescale calibration, osmium isotope seawater composition and Re–Os systematics in organic-rich sediments. *Chemical Geology*, **265**, 394–409.

Siewert, S.E. 2011. *Integrating $^{40}Ar/^{39}Ar$, U-Pb, and astronomical clocks in the Cretaceous Niobrara Formation*. MSc thesis, University of Wisconsin-Madison.

Singer, B.S., Jicha, B.R., Sawyer, D., Walaszczyk, I., Buchwaldt, R. and Mutterlose, J. 2021. Geochronology of late Albian–Cenomanian strata in the U.S. Western Interior. *Geological Society of America Bulletin*, **133**, 1165–1678, https://doi.org/10.1130/B35794.1

Sprain, C.J., Renne, P.R., Clemens, W.A. and Wilson, G.P. 2018. Calibration of Chron C29r: new high-precision geochronologic and paleomagnetic constraints from the Hell Creek Region, Montana. *Geological Society of America Bulletin*, **130**, 1615–1644, https://doi.org/10.1130/B31890.1

Walaszczyk, I. and Cobban, W.A. 2000. Inoceramid faunas and biostratigraphy of the Upper Turonian – Lower Coniacian of the Western Interior of the United States. *Special Paper in Palaeontology*, **64**, 1–118.

Walaszczyk, I. and Cobban, W.A. 2006. Palaeontology and biostratigraphy of the Middle–Upper Coniacian and Santonian inoceramids of the US Western Interior. *Acta Geologica Polonica*, **56**, 241–348.

Walaszczyk, I. and Cobban, W.A. 2007. Inoceramid fauna and biostratigraphy of the upper middle Coniacian–lower middle Santonian of the Pueblo Section (SE Colorado, US Western Interior). *Cretaceous Research*, **28**, 132–142, https://doi.org/10.1016/j.cretres.2006.05.024

Walaszczyk, I. and Cobban, W.A. 2016. Inoceramid bivalves and biostratigraphy of the upper Albian and lower Cenomanian of the United States Western Interior Basin. *Cretaceous Research*, **59**, 30–68, https://doi.org/10.1016/j.cretres.2015.10.019

Walaszczyk, I., Cobban, W.A. and Harries, P.J. 2001. Inoceramids and inoceramid biostratigraphy of the Campanian and Maastrichtian of the United States Western Interior basin. *Revue de Paléobiologie, Geneve*, **20**, 117–234.

Walaszczyk, I., Kennedy, W.J. and Klinger, H.C. 2009. Cretaceous faunas from Zululand and Natal, South Africa. Systematic palaeontology and stratigraphical potential of the Upper Campanian–Maastrichtian inoceramidae (Bivalvia). *African Natural History*, **5**, 49–132.

Walaszczyk, I., Plint, A.G. and Landman, N.H. 2017. Inoceramid bivalves from the Coniacian and basal Santonian (Upper Cretaceous) of the Western Canada Foreland basin. *Bulletin of the American Museum of Natural History*, **414**, 53–103, https://doi.org/10.1206/0003-0090-414.1.4

Walaszczyk, I., Čech, S. *et al*. (with contributions by Linnert, C., Püttmann, T., and Toshimitsu, S.) 2022. The Global Boundary Stratotype Section and Point (GSSP) for the base of the Coniacian Stage (Salzgitter-Salder, Germany) and its auxiliary sections (Słupia Nadbrzeżna, central Poland; Střeleč, Czech Republic; and El Rosario, NE Mexico). *Episodes*, **45**, 181–220, https://doi.org/10.18814/epiiugs/2021/021022

Zhu, Y., Bhattacharya, J.P., Li, W., Lapen, T.J., Jicha, B.R. and Singer, B.S. 2012. Milankovitch-scale sequence stratigraphy and stepped forced regressions of the Turonian Ferron Notom deltaic complex, south-central Utah, USA. *Journal of Sedimentary Research*, **82**, 723–746, https://doi.org/10.2110/jsr.2012.63